Renewable Energy 186 (2022) 927–943

Contents lists available at ScienceDirect

Renewable Energy

journal homepage: www.elsevier.com/locate/renene

# Techno-economic analysis of Advanced Geothermal Systems (AGS)

Adam E. Malek [a, *], Benjamin M. Adams [a], Edoardo Rossi [a], Hans O. Schiegg [b, **], Martin O. Saar [a, ***]

[a] Geothermal Energy and Geofluids Group, Department of Earth Sciences, ETH Zürich, Sonneggstrasse 5, 8092, Zürich, Switzerland
[b] SwissGeoPower Engineering AG, Breiteweg 37, 8707, Uetikon am See, Switzerland

ARTICLE INFO

*Article history:*
Received 5 May 2021
Received in revised form
15 December 2021
Accepted 4 January 2022
Available online 12 January 2022

*Keywords:*
Geothermal energy
Advanced geothermal systems
Closed-loop
Renewable energy
Electric power generation

ABSTRACT

Advanced Geothermal Systems (AGS) generate electric power through a closed-loop circuit, after a working fluid extracts thermal energy from rocks at great depths via conductive heat transfer from the geologic formation to the working fluid through an impermeable wellbore wall. The slow conductive heat transfer rate present in AGS, compared to heat advection, makes AGS uneconomical to this date. To investigate what would be required to render AGS economical, we numerically model an example AGS using the genGEO simulator to obtain its electric power generation and its specific capital cost. Our numerical results show that using $CO_2$ as the working fluid benefits AGS performance. Additionally, we find that there exists a working fluid mass flowrate, a lateral well length, and a wellbore diameter which minimize AGS costs. However, our results also show that AGS remain uneconomical with current, standard drilling technologies. Therefore, significant advancements in drilling technologies, that have the potential to reduce drilling costs by over 50%, are required to enable cost-competitive AGS implementations. Despite these challenges, the economic viability and societal acceptance potential of AGS are significantly raised when considering that negative externalities and their costs, so common for most other power plants, are practically non-existent with AGS.



## 1. Introduction

With efforts to meet the sustainable development goals set out by the Paris Agreement [1], global energy transition strategies have triggered the development of several technologies to generate electric power from renewable sources. The European Union aims to cover by 2050, using renewable energy sources, 60% of the gross energy consumption [2]. Intermittent energy sources, such as wind and solar, exhibit strong variability and non-linearity [3] and therefore cannot supply baseload power without requiring energy storage. Moreover, hydropower is limited to providing a potential 3.7 $TW_e$ of electric power, as it relies on site-specific conditions [4] and is therefore location-dependent. Therefore, there is an urgent need for an autarkic, location-independent, baseload and/or dispatchable, carbon-free energy source that can reliably meet heat and/or electric power demands.

Geothermal energy, the heat within Earth, corresponds to a potential of 40 $TW_{th}$ [5] which can be used, in part, to provide flexible and on-demand thermal and electrical power, thereby enabling a reliable baseload and even dispatchable power supply. Conventional geothermal energy generation from hydrothermal resources is a well-established field with competitive electricity prices.

One of the largest challenges when utilizing hydrothermal energy resources is to identify regions that exhibit sufficient natural reservoir permeability (due to connected pores and/or fractures and faults) and reservoir thickness (i.e., geologic reservoir transmissivity) to enable efficient, and thus economical, advective heat transport by circulating a fluid, typically water but potentially also carbon dioxide ($CO_2$) and other fluids (oil, gas) as discussed below, through the geologic reservoir. Thus, since the 1970s, the concept of Enhanced (or Engineered) Geothermal Systems (EGS), originally referred to as Hot Dry Rock (HDR) systems, has been contemplated and (partially) developed [6]. The idea of EGS is to drill and complete wells deep (5–7 km) into crystalline basement rock, where temperatures are high (>180°C) but where permeabilities are typically extremely low, and to artificially enhance the system's permeability through hydraulic stimulation. During hydraulic

* Corresponding author.
** Corresponding author.
*** Corresponding author.
*E-mail addresses:* amalek@ethz.ch (A.E. Malek), badams@ethz.ch (B.M. Adams), rossie@ethz.ch (E. Rossi), h.o.schiegg@bluewin.ch (H.O. Schiegg), saarm@ethz.ch (M.O. Saar).

https://doi.org/10.1016/j.renene.2022.01.012

**Nomenclature**

| | |
|---|---|
| $\alpha$ | Rock thermal diffusivity [mm$^2$ s$^{-1}$] |
| $\dot{m}$ | Working fluid mass flowrate [kg s$^{-1}$] |
| $\dot{m}^*$ | Optimal working fluid mass flowrate [kg s$^{-1}$] |
| $\Gamma$ | Thermal drawdown [−] |
| $\nabla T$ | Geothermal temperature gradient [°C km$^{-1}$] |
| $\dot{W}$ | Power [W] |
| $\rho_{rock}$ | Rock density [kg m$^{-3}$] |
| $c_{p,rock}$ | Rock specific heat capacity [J °C$^{-1}$kg$^{-1}$] |
| $k_{rock}$ | Rock thermal conductivity [W$_{th}$ °C$^{-1}$m$^{-1}$] |
| $L_{LW}$ | Lateral well length [km] |
| $L^*_{LW}$ | Optimal lateral well length [km] |
| $q_{pipe-fluid}$ | Heat flux, from wellbore to working fluid [W$_{th}$ m$^{-2}$] |
| $Q_{rock-pipe}$ | Heat flux, from rock to wellbore [W$_{th}$ m$^{-2}$] |
| $T$ | Rock temperature [°C] |
| $z$ | Depth [km] |

*Subscripts*

| | |
|---|---|
| e | electrical |
| r | radial distance from the wellbore |
| th | thermal |
| wall | wellbore wall |
| well, h | horizontal wellbore |
| well, v | vertical wellbore |

*Abbreviations*

| | |
|---|---|
| AGS | Advanced geothermal systems |
| CC | Capital cost [2019$] |
| CPG | $CO_2$ plume geothermal |
| CTMD | Combined thermo-mechanical drilling |
| EGS | Enhanced (or engineered) geothermal systems |
| GHG | Greenhouse gas |
| LCOE | Levelized cost of electricity |
| ORC | Organic Rankine cycle |
| SpCC | Specific capital cost [2019$ $W_e^{-1}$] |

stimulation, large quantities of water are injected under high pressure into the low-permeability rock formation either generating new fractures (hydraulic fracturing or fracking) or reactivating critically stressed pre-existing fractures or faults (hydraulic shearing) or both [7,8]. As a result, the technology induces at least small earthquakes [9–12] and the created flow paths are prone to being sealed due to geochemical reactions between the rock and the water leading to mineral scaling [13–17]. Research efforts are, however, under way to reduce and, ideally, eliminate both large earthquakes and mineral scaling [18,19].

Conversely, $CO_2$ Plume Geothermal (CPG) utilizes $CO_2$ as the subsurface working fluid in naturally-permeable sedimentary rock formations, which doubles or triples its efficiency, compared to water underground [20–23]. While CPG dramatically improves the efficiency of geothermal energy extraction and utilization, enabling lower resource temperatures to be used economically, it still requires naturally permeable formations, like other hydrothermal systems, albeit much lower natural permeabilities (or transmissivities) can be used for economic CPG-based power generation than for water-based systems [20,22]. Thus, CPG is still a hydrothermal system, however, its implementation is economically possible at many more locations worldwide than water-based hydrothermal systems, due to CPG's less stringent reservoir temperature and permeability requirements [22]. Nonetheless, suitable geologic reservoirs need to be found for CPG as well. Thus, CPG implementation still depends on the local geology, where geologic $CO_2$ sequestration must be possible at reservoir depths of at least about 2 km and associated CPG-enabling temperatures, unless for example additional heating of the produced working fluid occurs in so-called hybrid geothermal power systems [24].

All the aforementioned geothermal power systems are open systems, where the subsurface working fluid is in direct contact with the surrounding rock, and therefore they all have additional drawbacks including: high regulatory barriers for their installation [25], potential of fluid loss in the reservoir [26,27], and mineral scaling [17].

Advanced Geothermal Systems (AGS) generate heat and/or electric power through a closed-loop circuit, after a working fluid, such as water or $CO_2$, extracts thermal energy from rock formations at great depths via conductive heat transfer from the geologic formation to the working fluid in the closed loop through an impermeable zone, such as a pipe wall. The deep rock formations accessed by AGS may be sedimentary rocks or, ideally, even deeper and thus hotter crystalline rock formations. As the subsurface working fluid within the closed loop never comes into direct contact with the surrounding rock, the above problems arising from subsurface open-loop geothermal system operations are practically eliminated. Additionally, AGS do not require many site-specific conditions and can therefore be deployed virtually anywhere, as long as the drilling and completion of the wells in both vertical and horizontal directions is economically feasible, given the local geology. This latter part, i.e., the high costs of vertical and horizontal well drilling, particularly at great depths and ideally in crystalline rocks, is therefore also the main disadvantage of AGS. Reducing the well drilling and completion costs significantly is so important to enable economical AGS implementations, as conductive heat transfer from the geologic formation to the working fluid (situated in the closed loop) through an impermeable zone, such as a pipe wall, is extremely slow, compared to heat advection.

AGS represent a novel power plant technology and therefore little to no research on AGS performance is available. In particular, the cost of capital expenditure per unit of electric power (or specific capital cost) of a conduction-based geothermal system, such as AGS, has not yet been published to the best of our knowledge, with exception of a recent paper by the authors [28]. For example, van Oort et al. [29] investigate only the short-term thermal power potential of AGS without considering the heat depletion of the geothermal reservoir. In Song et al. [30], a model is presented for the circulation of a water subsurface working fluid in a U-shaped wellbore configuration that consists of two vertical wells and a single lateral well. The model is used to determine the production temperature of the working fluid at several operating parameters, including the water mass flowrate and its inlet temperature, the length of the horizontal section, and the wellbore diameter. Esmaeilpour et al. [31] extend the analysis to include the effects of vertical well depth and rock thermal conductivity on the production temperature and thermal power. In contrast, Sun et al. [32] employ $CO_2$ as the subsurface working fluid in the U-shaped wellbore configuration model, with the goal of determining the $CO_2$ temperature and pressure profiles. In Wang et al. [33], a water working fluid is circulated through a coaxial multilateral wellbore system consisting of a single vertical wellbore and several horizontal wellbores. Each wellbore functions as both an injection and a production well, consisting of an outer and an inner pipe. The analysis is based on determining the effects of varying different operating parameters on the working fluid production temperature and thermal power.

To economically generate utility-scale electric power in regions with average subsurface temperatures, AGS requires vertical wells which extend to depths beyond 5.0 km, where the rock temperature is high [29]. However, drilling to such large depths using state-of-the-art drilling technologies is technically difficult and economically prohibitive [34–36].

Hence, AGS is currently economically non-viable due to the large costs associated with well development. For AGS to be economically viable and able to compete with other renewable energy generation technologies, its specific capital cost (SpCC) must be in the range of 2.0–5.0 2019$ $W_e^{-1}$ [37]. However, most studies, such as IRENA (p. 45, 136 in Ref. [37]), do not consider the monetary impact of air pollution, environmental contamination, impacts on the local landscape, amongst other negative externalities, from using other energy generation technologies. In contrast to all other power supply sources, little to no negative externalities are associated with AGS, thereby raising the technology's economic viability and likelihood of societal acceptance.

This paper therefore serves as a novel work which aims at simulating a range of example AGS with the goal of quantifying their long-term performance, in particular their electric power generation potential and associated costs after 30 years of operation. Both water and $CO_2$ are used as the subsurface working fluids in the various AGS for a wide range of system depths, lateral well lengths and configurations, wellbore diameters, and geologic conditions. These results assist in evaluating the feasibility of AGS development and operation, as the first AGS projects are being developed already throughout the world.

## 2. Method

### 2.1. Simulation method for electric power and cost

This paper aims at examining the performance of Advanced Geothermal Systems (AGS) (i.e., electric power and cost) by employing 'genGEO' [38] as the software for all system simulations. As geothermal electricity generation simulations first require geothermal heat extraction simulations, we do not explicitly discuss the heat extraction performance of AGS here.

The characteristics of 'genGEO' are described in a recent publication [38]. genGEO, available as an open-source python library, is a generalizable geothermal simulator, which is used as a techno-economic tool for determining the electric power and cost of a wide range of geothermal systems. Although several other geothermal techno-economic tools exist (i.e., GEOPHIRES [39], GETEM [40]), genGEO is chosen for this study since its generalizability allows us to use it for AGS, with only having to implement few modifications.

genGEO is an integrated simulator, composed of a reservoir model which simulates the working fluid's energy and pressure change in the porous reservoir, a well model which simulates the working fluid's energy and pressure change in the wellbores, a thermodynamic power cycle model which simulates electric power generation, and a cost model which evaluates the capital costs. Adams et al. [38] applied genGEO to sedimentary basin geothermal power plants, which extract heat from a porous reservoir.

We construct the AGS model, used in this work, by replacing the porous and/or fractured reservoir, present in sedimentary basin geothermal systems, with one or several horizontal lateral wells, which interact with the surrounding rock through heat conduction. The conductive heat exchange wellbore model is already employed by the vertical wells, and is therefore extended to these horizontal lateral wells. For a more detailed description of the heat exchange between the fluids in the wellbore and the surrounding rock, the reader is referred to Adams et al. [38] and Zhang et al. [41]. Furthermore, the working fluid mass flowrate in each lateral well is the mass flowrate in each of the vertical wells divided by the number of lateral wells.

### 2.2. Model description

The Advanced Geothermal System (AGS) shown in Fig. 1 is simulated with either water or (supercritical) $CO_2$ as the subsurface working fluid in the closed loop, which receives heat via thermal conduction from the rock formation surrounding the closed-loop. Our AGS model consists of a geothermal doublet, where two vertical wellbores are drilled from the surface to a targeted depth. One wellbore is used as an injection well to deliver the cooled working fluid to the targeted depth, while the other is used as a production well which withdraws the hot working fluid and delivers it to the surface power plant to produce electricity. The vertical wells are connected at the targeted depth by one or several horizontal lateral wells, thereby closing the loop and allowing the working fluid to circulate.

The power plant configuration depends on the working fluid circulated in the closed subsurface loop. The power cycle is either a direct system, where $CO_2$ is directly expanded in a surface turbine, or an indirect system, where heat is extracted from the water to drive a secondary organic Rankine cycle (ORC) [22]. The latter uses R245fa as the secondary working fluid. All surface power plant parameters are based on estimated performance data from turbine and pump manufacturers [22]. The main assumptions of the AGS model are shown in Table 1.

A well success rate of 95% is used for AGS. Ref. [39,40] use success rates of 100% and 90%, respectively, for deep EGS developments, and therefore the middle value is selected. The success rate of this technology is not well known, as very few geothermal installations have been developed to large depths in crystalline rocks, and may thus underestimate actual drilling conditions and associated costs in crystalline basement rocks.

#### 2.2.1. Base-case parameters

Several base-case parameters were selected to constitute a reference scenario and are listed in Table 2. These parameters serve as the model input variables and are categorized into operating parameters or geologic conditions. The definition of a reference scenario is advantageous, as its results serve as a useful benchmark for comparing how varying the system parameters affects the electricity generation and cost results (Section 3).

The operating parameters relate to the controlled inputs, such as the working fluid type, its mass flowrate, $\dot{m}$, or the size and length of the wellbores. The operating parameters chosen for the base-case AGS considered here include four 5.0 km long lateral wells, connected at a depth of 3.5 km by the vertical wellbores. Provided that the wellbore spacing is large enough to limit thermal interference between the wellbores (Section 2.2.2), the power and cost results are independent of the geometrical layout of the lateral wells. Furthermore, an admittedly large wellbore diameter of 0.50 m is used for the reference scenario. However, this large well diameter is reduced considerably for alternative AGS realizations, should modern, contact-less drilling technologies, currently under development (see references in Section 4.2) not be able to provide such large-diameter wells at significantly reduced costs as currently anticipated. It should also be mentioned that smaller well diameters are even preferred if the wellbores are limited to shallow vertical well depths, as discussed in Section 4.1.

The geologic conditions relate to the intrinsic aspects of the geology of the region, such as geothermal gradient, $\nabla T$, or rock thermal conductivity, $k_{rock}$. To be consistent with the base-case

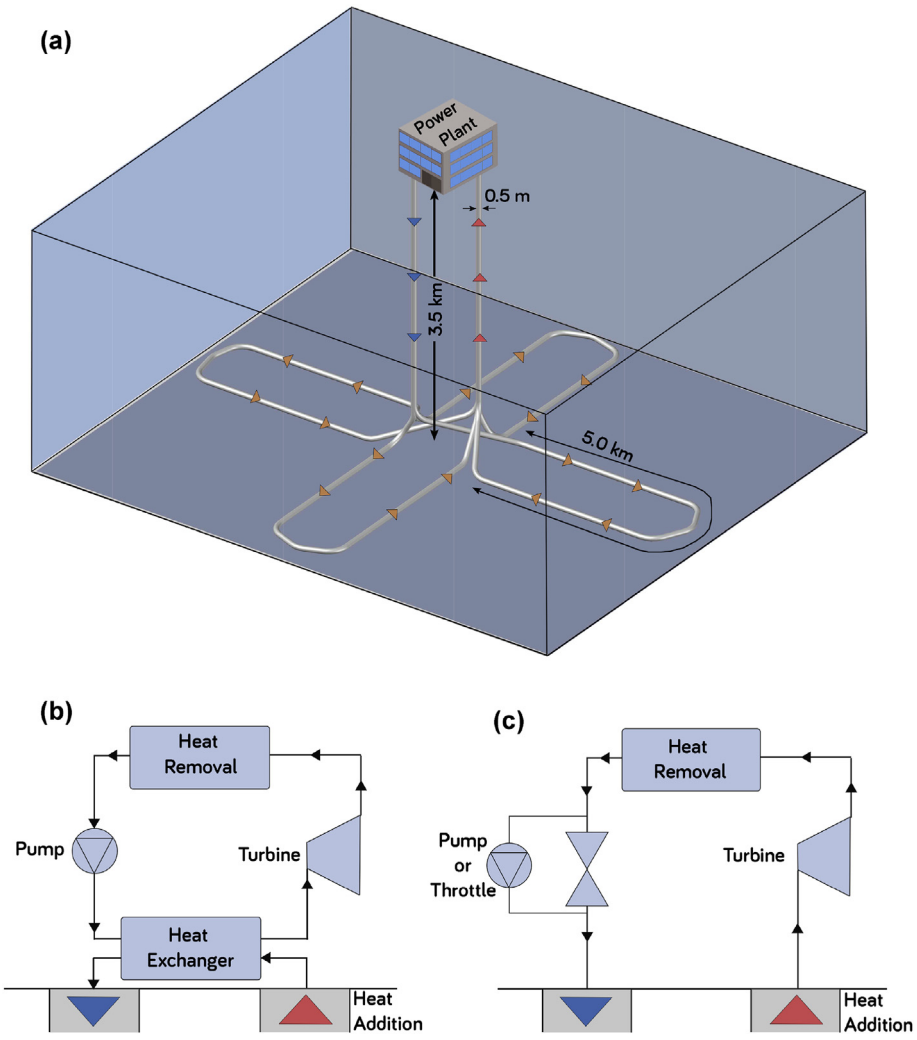


**Fig. 1.** Schematic representation of the AGS base case system modeled here. (a) shows the surface power plant, the geothermal reservoir, the 3.5 km vertical wells, and the four 5.0 km lateral wells. The electric power and cost results are independent of the lateral well configuration, as long as there is sufficient spacing between them (Section 2.2.2). The electricity in the power cycle is generated either by (b) an organic Rankine cycle (ORC), if water is used as the subsurface working fluid, or (c) directly in a surface turbine, if $CO_2$ is used as the subsurface and surface working fluid in a single cycle. The working fluid's direction of travel is indicated by the colored arrows.

**Table 1**
Main AGS model assumptions.

| Parameter | Assumed value |
|---|---|
| Surface power plant parameters | |
| Turbine isentropic efficiencies | |
| *for water system* | 0.8 |
| *for $CO_2$ system* | 0.78 |
| Pump isentropic efficiencies | |
| *for water system* | 0.9 |
| *for $CO_2$ system* | 0.9 |
| ORC Fluid | 1,1,1,3,3-Pentafluoropropane (R245fa) |
| Financial parameters | |
| Geothermal plant layout | Greenfield |
| Well success rate | 0.95 |
| Duration of thermal depletion | 30 [years] |
| Water downhole pump depth | 0.5 [km] |
| Water downhole pump efficiency | 0.75 |
| Well pipe roughness | 55 [$\mu$m] [42] |

**Table 2**
Base-case model parameters.

| Parameter | Value |
|---|---|
| Operating parameters | |
| Number of injection wells | 1 |
| Number of production wells | 1 |
| Number of lateral wells | 4 |
| Length of vertical wells | 3.5 [km] |
| Length of lateral wells | 5.0 [km] |
| Well diameter | 0.5 [m] |
| Subsurface working fluid | Water (ORC) or $CO_2$ |
| Geologic Conditions | |
| Mean annual land surface air temperature | 15 [°C] |
| Geothermal gradient | 35 [°C km$^{-1}$] |
| Rock density | 2650 [kg m$^{-3}$] |
| Specific heat capacity | 1000 [J °C$^{-1}$ kg$^{-1}$] |
| Thermal conductivity | 2.1 [$W_{th}$ °C$^{-1}$ m$^{-1}$] |
| Thermal diffusivity | 0.79 [mm$^2$ s$^{-1}$] |

study parameters used in Ref. [38], the geothermal gradient, assumed to be constant with depth, is 35 °C km$^{-1}$. As an example, the average geothermal gradient in the western United States is 34 °C km$^{-1}$ [43].

Due to the large target depths of AGS, the geothermal reservoir is assumed to be composed of a homogeneous, isotropic crystalline rock. Typical values for thermal conductivity, $k_{rock}$, and specific heat capacity, $c_{p,rock}$, of crystalline basement rocks are 2.8–3.5

$W_{th}\,°C^{-1}\,m^{-1}$ [44] and 700–1000 J $°C^{-1}\,kg^{-1}$ [45], respectively. Both properties are temperature-dependent, and are therefore assumed to be 2.1 $W_{th}\,°C^{-1}\,m^{-1}$ and 1000 J $°C^{-1}\,kg^{-1}$ for this study, due to the subsurface rock temperatures being high. Additionally, a rock density, $\rho_{rock}$, of 2650 kg $m^{-3}$ is used for this study [46]. The rock thermal diffusivity, $\alpha$, of 0.79 $mm^2\,s^{-1}$, is determined from Equation (1),

$$\alpha = \frac{k_{\text{rock}}}{\rho_{\text{rock}}\, c_{\text{p, rock}}}. \tag{1}$$

### 2.2.2. Duration of thermal depletion and its implications for wellbore spacing

The time-dependent thermal depletion of the hot formation decreases the amount of thermal energy the AGS can use to generate electricity. A time-dependent thermal drawdown is the result of the conductive heat transfer from the far-field hot rock into the working fluid in the wellbore.

Carslaw and Jaeger [47] developed a semi-analytic solution for radial conductive heat flow to calculate the temperature distribution between a cylinder and the surrounding media. The thermal drawdown, $\Gamma_r$, at a specified depth and radial distance, $r$, from the center of the wellbore is given in Equation (2). $T_r$, $T_{\text{wall}}$, and $T_{\text{surrounding}}$ represent the temperatures at the specified radial distance, the wellbore wall, and in the far-field surroundings, respectively. $T_{\text{surrounding}}$ is found by multiplying the depth by the geologic temperature gradient, and adding the mean annual land surface air temperature. At the base-case depth of 3.5 km, $T_{\text{surrounding}}$ is 137.5 °C.

$$\Gamma_r = \frac{T_r - T_{\text{surrounding}}}{T_{\text{wall}} - T_{\text{surrounding}}} \tag{2}$$

Fig. 2, adapted from Ref. [47] for a wellbore radius of 0.50 m and a thermal diffusivity of 0.79 $mm^2\,s^{-1}$, outlines the time-dependent thermal drawdown, $\Gamma_r$. The colored curves represent the amount of time since the onset of thermal depletion, i.e., the start of AGS operations.

The thermal depletion decreases with radial distance from the wellbore. After 2.5 years, $\Gamma_r = 0.3$ for the rock at a radial distance of 4 m, whereas the rock 25 m away is unaffected.

Similarly, the thermal depletion increases with time. At a radial distance of 4 m, $\Gamma_r = 0.1$ after 0.25 years, and increases to $\Gamma_r = 0.3$ after 2.5 years.

As expected, the rate of thermal depletion decreases with time. At a radial distance of 1 m, the rock undergoes a 30% change in thermal depletion over the first 9 days of AGS operation, which decreases to only a 5% increase in the time between 0.75 years and 2.5 years. We expect that the change in the rate of thermal depletion is negligible after 30 years of operation. Thus, the electric power that the AGS is capable of generating is shown after 30 years of thermal depletion. Using less than this duration will overestimate the amount of electric power generation that an AGS will generate over its lifetime.

Furthermore, the wellbores must be adequately spaced apart so that there is negligible thermal influence between them. We consider the radius of thermal influence to be the radial distance from a wellbore, where the thermal depletion is 5% of its initial value, marked by the dashed black line in Fig. 2. Ref. [47] only provide the thermal depletion values for the first 2.5 years. Therefore, we extrapolate the 30-year value, and find a radius of thermal influence of 38 m for the base-case AGS (marked by the star in Fig. 2). Thus, the wellbores must be separated by at least 76 m in our case. If smaller well diameters are used, or if a thermal depletion of more than 5% is considered to be tolerable, smaller wellbore spacings may be implemented.

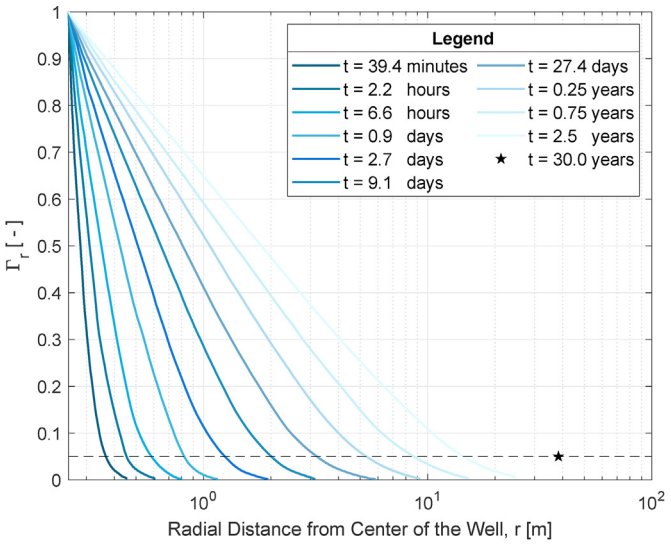


**Fig. 2.** Thermal drawdown of the hot rock formation for different heat conduction durations as a function of radial distance from the center of the well. The thermal drawdown, $\Gamma_r$, is the ratio of the temperature at the specified radial distance from the well and the temperature at the wellbore wall. The predicted radial distance from the center of the well, which has a 5% thermal drawdown after 30 years of AGS operation, is 38 m, as indicated by the star (base-case AGS). The figure is adapted from Ref. [47] for a well diameter of 0.50 m and a thermal diffusivity of 0.79 $mm^2\,s^{-1}$.

### 2.3. Electricity generation and cost metrics used to evaluate AGS performance

We evaluate the performance of the Advanced Geothermal System (AGS) shown in Fig. 1 using the electricity generation and cost produced by its simulation in genGEO. The performance metrics we use to assess the electricity generation and cost are the electric power, $W_e$, the specific electric power, the capital cost (CC), and the specific capital cost (SpCC).

The main function of an AGS is to provide electricity (and/or heat). The total electric power generated, $W_e$, is equal to the gross turbine output less the parasitic electric loads (e.g., cooling towers and pumping, if needed, which may not be needed when $CO_2$ is used as the working fluid [21]). Furthermore, the specific electric power, defined as the electric power divided by the total wellbore length [$W_e\,m^{-1}$], is used to identify the impact that the total drilled wellbore length has on the electricity generated. The total wellbore length of the base-case scenario consisting of two 3.5 km-deep vertical wells and four 5.0 km-long lateral wells is 27 km.

The capital cost (CC) of the system is the total overnight cost to construct the entire AGS facility. This includes the cost of drilling and well completion, wellfield development, surface piping, and the cost of developing the surface power plant. Further information on how these costs are quantified can be found in the 'genGEO' publication [38].

Moreover, the capital cost calculation in 'genGEO' is modified for the closed-loop AGS. This is done by reducing the wellfield costs to only include the permitting cost required for developing the wells, and by eliminating the exploration and development costs that are otherwise always included in open geothermal systems. Also, the capital cost calculation is modified to include the additional cost of developing the horizontal lateral wells, $CC_{\text{well, h}}$, at the targeted

depth, $z$. The cost of developing the vertical wells, $CC_{well,\,v}$, already included in genGEO, is used to develop the $CC_{well,\,h}$ cost function. As illustrated by Equation (3), this is done by taking the difference between the cost of a vertical well with a length of the targeted depth, $z$, plus half the lateral well length, and the cost of a vertical well with a length of $z$,

$$CC_{well,\,h}(L_{LW}) = CC_{well,\,v}(z + 0.5 \cdot L_{LW}) - CC_{well,\,v}(z). \quad (3)$$

Finally, the specific capital cost (SpCC) provides the cost required to produce a unit of electric power [$\$\,W_e^{-1}$], as shown in Equation (4). The SpCC combines all the other aforementioned electric power and cost metrics. Thus, the SpCC is minimized for optimal AGS performance and is given by

$$SpCC = \frac{CC_{AGS}}{\bar{W}_e}, \quad (4)$$

where $CC_{AGS}$ is the capital cost of the entire AGS.

All cost calculations in genGEO include either 'baseline' or 'ideal' well cost assumptions, first introduced by Ref. [48]. The 'baseline' costs represent the costs resulting from state-of-the-art drilling technologies. The recent state of geothermal drilling technology is comprehensively summarized in Ref. [49]. Conversely, 'ideal' costs represent a theoretical minimum in drilling and completion costs that would be obtained if significant advancements in drilling technology occurred. All costs reported in the subsequent sections are baseline costs, unless explicitly stated otherwise.

Additionally, all costs provided are 2019 US dollars and are shown as [$]. Also, all performance metrics described above are found from the base case parameters, summarized in Table 2, unless explicitly stated otherwise.

To summarize, the procedure for determining the electric power generation and cost metrics, along with the input parameters which are varied in several scenarios in Section 3, is presented schematically in Fig. 3.

## 3. Results

The performance of an Advanced Geothermal System (AGS) is influenced by various operating parameters and geologic conditions. In this section, we report the results of several parametric studies employing genGEO for different scenarios. Firstly, in Section 3.1, we investigate using water and $CO_2$ as the subsurface working fluids in the closed loop and how they affect the performance of the system. Afterwards, we investigate the AGS performance by varying several operating parameters of the system. Specifically, we report the results obtained by varying the horizontal lateral well lengths from 0 to 30 km in Section 3.2, by varying the number of horizontal lateral wells from 1 to 8 in Section 3.3, and also for wellbore diameters of 4 inches, 6 inches, $9^{5/8}$ inches, and 0.50 m in Section 3.4. Lastly, to investigate the effect of the geologic conditions on AGS performance, sensitivity analyses are performed for various geothermal gradients (Section 3.5) and rock thermal conductivities (Section 3.6).

### 3.1. Base case results and effect of subsurface fluid type on AGS performance

Fig. 4 shows the electric power, production temperature, specific electric power, and SpCC results for both subsurface water and $CO_2$ circulated through the base-case AGS at mass flowrates, $\dot{m}$, varying between 0 and 100 kg $s^{-1}$.

We observe a convex shape of the SpCC curves for each working fluid, which suggests the existence of a cost-minimizing mass flowrate, $\dot{m}$, represented by the stars in Fig. 4. The electric power is maximized at a different, albeit similar, $\dot{m}$, that minimizes the SpCC. Although the values are different, the former is used as the optimal mass flowrate, $\dot{m}^*$, since it gives the most economical output. Table 3 shows the $\dot{m}^*$ for each subsurface working fluid type and the corresponding electric power and cost results generated by circulating the working fluid at its corresponding $\dot{m}^*$.

We find that operating $CO_2$ as the working fluid at $\dot{m}^* = 53.0$ kg $s^{-1}$, rather than operating water at $\dot{m}^* = 26.7$ kg $s^{-1}$, results in higher electricity generation and in a smaller SpCC. It is therefore assumed that using $CO_2$ will result in more optimal power and cost outputs for all scenarios and input conditions examined throughout the remainder of Section 3. Thus, we henceforth only report the results for an AGS operating continuously with the $CO_2$ working fluid at the corresponding $\dot{m}^*$, unless explicitly stated otherwise.

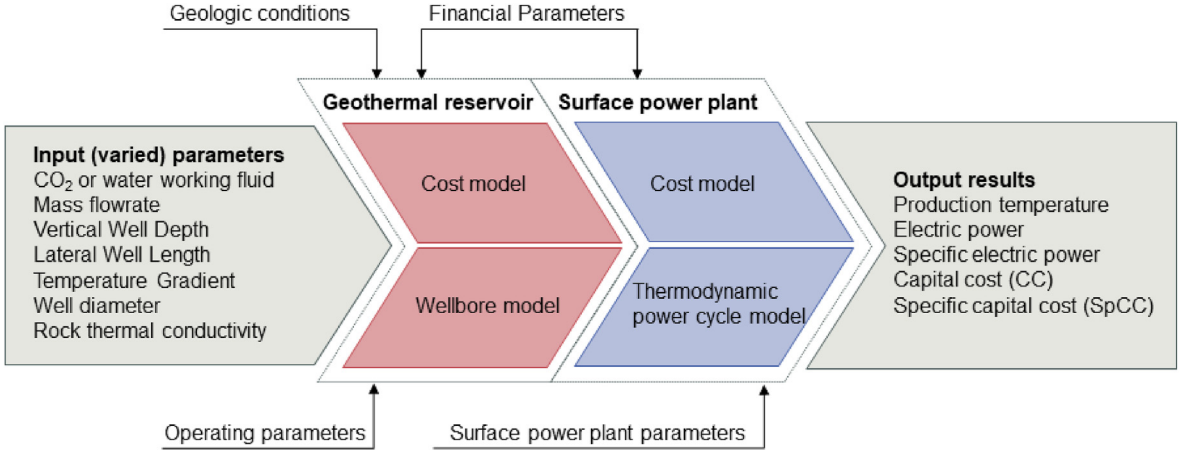


**Fig. 3.** Scheme of the genGEO calculation process, which converts the input parameters into a set of electricity generation and cost metrics. Each of the input parameters shown are varied for the different scenarios discussed in Section 3. Given these inputs, genGEO simulates the entire AGS using a conductive heat exchange wellbore model, a thermodynamic power cycle model, and a cost model, shown in red and blue for the geothermal reservoir and surface power plant blocks, respectively. Each block employs a set of financial and surface power plant assumptions (detailed in Table 1) and the remaining operating and geologic parameters (detailed in Table 2), which are shown by the black arrows in the present Fig. 3.

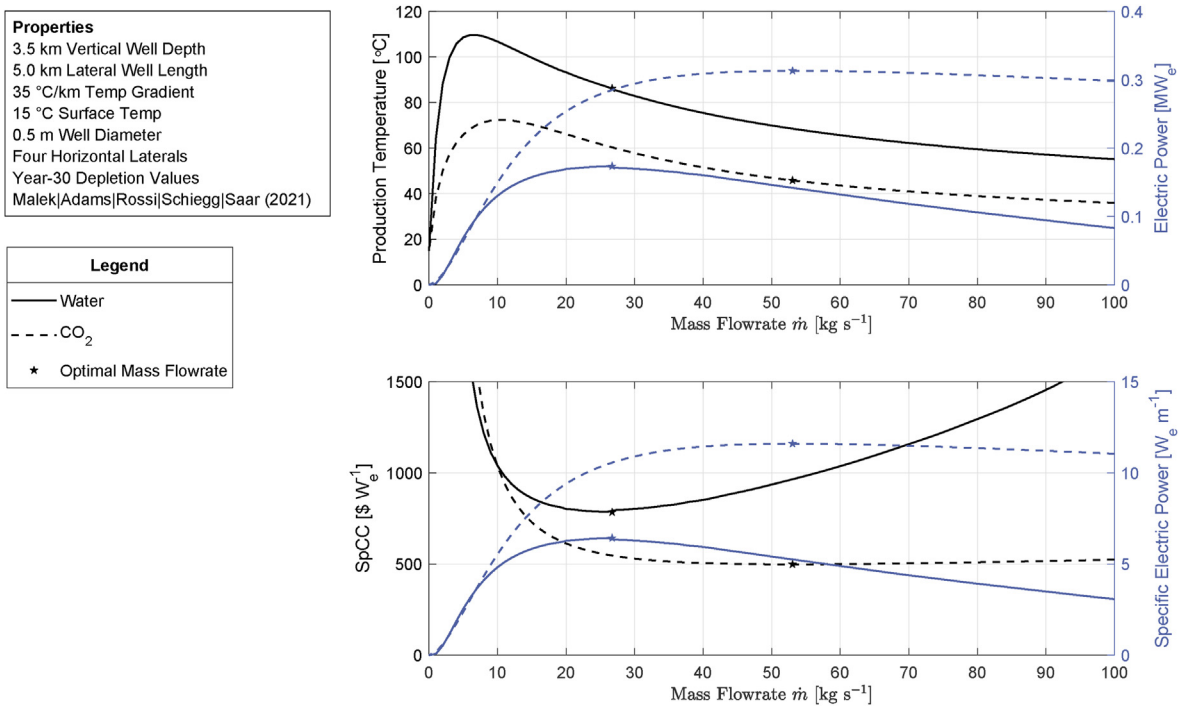


**Fig. 4.** AGS performance for subsurface water (solid lines) and $CO_2$ (dashed lines) working fluid mass flowrates of 0–100 kg $s^{-1}$. The black lines (production temperature at the top and SpCC at the bottom) and blue lines (electric power at the top and specific electric power at the bottom) are shown on the left and right y-axes, respectively. The stars indicate the mass flowrate resulting in a minimum SpCC.

**Table 3**
Base case results.

| | Water | $CO_2$ |
|---|---|---|
| Optimal Mass Flowrate, $\dot{m}^*$ [kg $s^{-1}$] | 26.7 | 53.0 |
| Power Generated [$kW_e$] | 174.0 | 313.0 |
| Production Temperature [°C] | 86.2 | 45.8 |
| Specific Power [$W_e$ $m^{-1}$] | 6.4 | 12.0 |
| 'Baseline' Capital Cost [M$] | 136 | 156 |
| 'Ideal' Capital Cost [M$] | 50 | 70 |
| 'Baseline' Specific Capital Cost (SpCC) [$ $W_e^{-1}$] | 785 | 498 |
| 'Ideal' Specific Capital Cost (SpCC) [$ $W_e^{-1}$] | 290 | 224 |

### 3.2. Effect of wellbore lengths and ideal cost assumptions on AGS performance

Fig. 5 shows the effect that varying the length (i.e., depth) of the vertical wells from 1 to 8 km, and varying the length of the horizontal lateral wells from 0 to 30 km has on the SpCC, electric power, specific electric power, and production temperature.

The concavity of the SpCC contours suggests the existence of a cost-minimizing lateral well length, $L^*_{LW}$, at each vertical well depth, represented by the blue lines in Fig. 5a. This optimal lateral well length increases with depth, for the selected input parameters.

We also find that assuming 'ideal' well costs (shown as dashed black contours in Fig. 5a) decreases the SpCC of the system. 'Ideal' well cost assumptions, first introduced by Ref. [48], assume significant advancements in drilling technology. Conversely, 'baseline' costs (shown as solid black contours) are representative of current state-of-the-art drilling technology. Since the cost function of the 'ideal' scenario is different, the $L^*_{LW}$ is also different, regardless of whether all other parameters are identical or not. Both 'baseline' and 'ideal' cost assumptions assume employing rotary drilling technologies. All costs reported in this paper are 'baseline' costs, unless explicitly stated otherwise.

At the base-case vertical well depth of 3.5 km, an optimal lateral well length of 5.9 km results in an electric power of 364 $kW_e^{-1}$ and an SpCC of 497 $\$W_e^{-1}$. The SpCC further reduces to 193 $\$W_e^{-1}$ if 'ideal' costs are used with an optimal lateral well length of 18.4 km.

### 3.3. Effect of the number of lateral wells on AGS performance

Fig. 6 illustrates the influence that varying the number of horizontal lateral wells, from 1 to 8, has on SpCC, specific electric power, electric power, and production temperature. As can be observed, increasing the number of horizontal lateral wells significantly benefits the electric power and SpCC results. Interestingly, large changes of electric power generation occur at approximately constant working fluid production temperatures. Increasing the number of lateral wells corresponds to a larger optimal mass flowrate, $\dot{m}^*$, and a smaller optimal lateral well length, $L^*_{LW}$. These changes result in the working fluid being produced at relatively constant production temperatures. At the vertical well depth of 3.5 km, the electricity produced is increased from 367 $kW_e$ to 1008 $kW_e$ by increasing the number of lateral wells from 1 to 8. This corresponds to only a 3 °C increase in fluid production temperature.

### 3.4. Effect of the wellbore diameter on AGS performance

Fig. 7 presents the electric power and SpCC results for 4-, 6-, and $9^{5/8}$-inch and 0.50 m well diameters. Geothermal wellbore diameters are commonly $9^{5/8}$-inches [50–52], but may also be smaller or alternatively extend up to 0.50 m diameters in extreme cases. Thus, we set the 4-inch and 0.50 m wellbore diameters as our minimum and maximum limits for our study.

As shown in Fig. 7b, increasing the wellbore diameter results in a notably higher electric power generated. Additionally, the amount of electricity generated when using larger wells increases

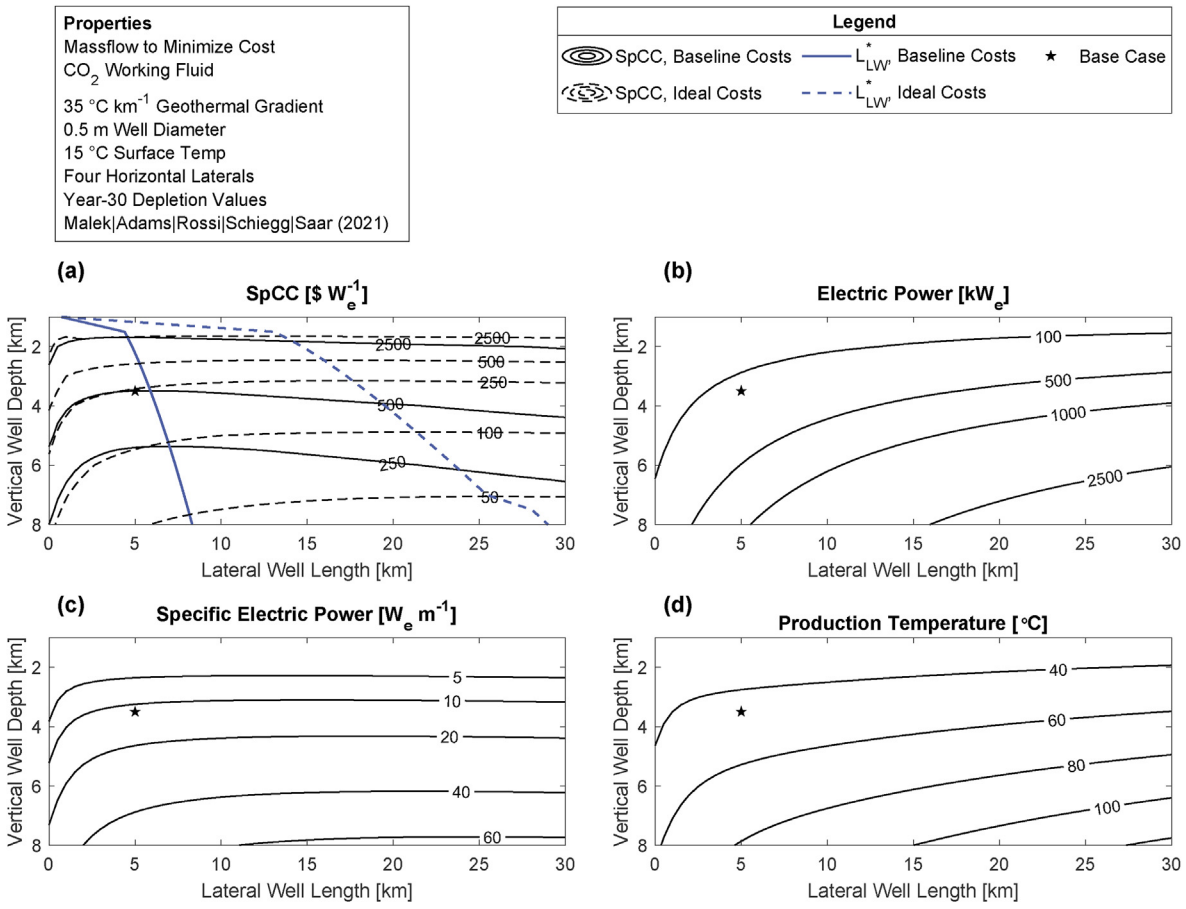


**Fig. 5.** Effect of various vertical and lateral well lengths on AGS performance. (a) shows the effect of using 'baseline' costs (solid black contours) and 'ideal' costs (dashed black contours) on the specific capital cost (SpCC), i.e., the cost required to produce a unit of electric power. For every vertical well depth, the optimal lateral well length, $L^*_{LW}$, that minimizes the SpCC, is indicated by the blue lines in (a). The electric power, specific electric power, and working fluid production temperature results are shown in (b), (c), and (d), respectively. The stars indicate the outputs from the base case.

more sharply with increasing vertical well depth. This results in substantially higher electric power values at large vertical well depths. For instance, for a 8.0 km vertical well depth, switching from the 4-inch well diameter to the 0.50 m well diameter changes the electric power from 360 $kW_e$ to 2820 $kW_e$.

The drilling and completion costs are dependent on the wellbore diameter. Indeed, a larger well diameter also increases the drilling and completion costs. Thus, a larger well diameter does not imply a lower SpCC. This suggests the existence of a cost-minimizing well diameter.

### 3.5. Effect of the geologic temperature gradient on AGS performance

Fig. 8 presents the electric power and SpCC results for 25, 30, 35, and 40 °C $km^{-1}$ geologic temperature gradients, $\nabla T$. We find that higher geologic temperature gradients transfer the electric power and cost to more optimal states. For example, at a 3.5 km vertical well depth, an increase in the geologic temperature gradient from 35 to 40 °C $km^{-1}$ corresponds to a 34% increase in electric power produced and a 24% decrease in SpCC. This highlights the need for accurate geologic temperature gradient measurements to successfully predict the performance of any AGS development. Additionally, there are clear advantages in locating AGS developments in geothermally active zones.

Interestingly, the optimal mass flowrate, $\dot{m}^*$, and the optimal lateral well length, $L^*_{LW}$ are generally constant, regardless of the geologic temperature gradient. These parameters vary by no more than 19% and 10%, respectively, for any vertical well depth larger than 3.5 km.

### 3.6. Effect of the rock thermal conductivity on AGS performance

The results showing the effect of the rock thermal conductivity, $k_{rock}$, on the AGS performance are presented in Fig. 9. In the following, $k_{rock}$ values in the range from 2.1 to 3.5 $W_{th}\,°C^{-1}\,m^{-1}$ are investigated. These are common thermal conductivity values for crystalline basement rock [44].

As shown in Fig. 9b, an increase in $k_{rock}$ translates to higher electric power generated and to lower SpCC values. For instance, at a 3.5 km vertical well depth, increasing the rock thermal conductivity from 2.1 to 2.8 $W_{th}\,°C^{-1}\,m^{-1}$ leads to the electric power increasing from 364 to 464 $W_e$ and to the SpCC reducing from 497 to 385 $\$\,W_e^{-1}$. This highlights the importance of accurately measuring subsurface thermal conductivities when attempting to predict AGS performance.

Furthermore, the optimal lateral well length, $L^*_{LW}$, remains approximately constant for any change in rock thermal conductivity. For the $k_{rock}$ values considered in this paper, $L^*_{LW}$ varies by no more than 5% for any vertical well depth up to 8 km.

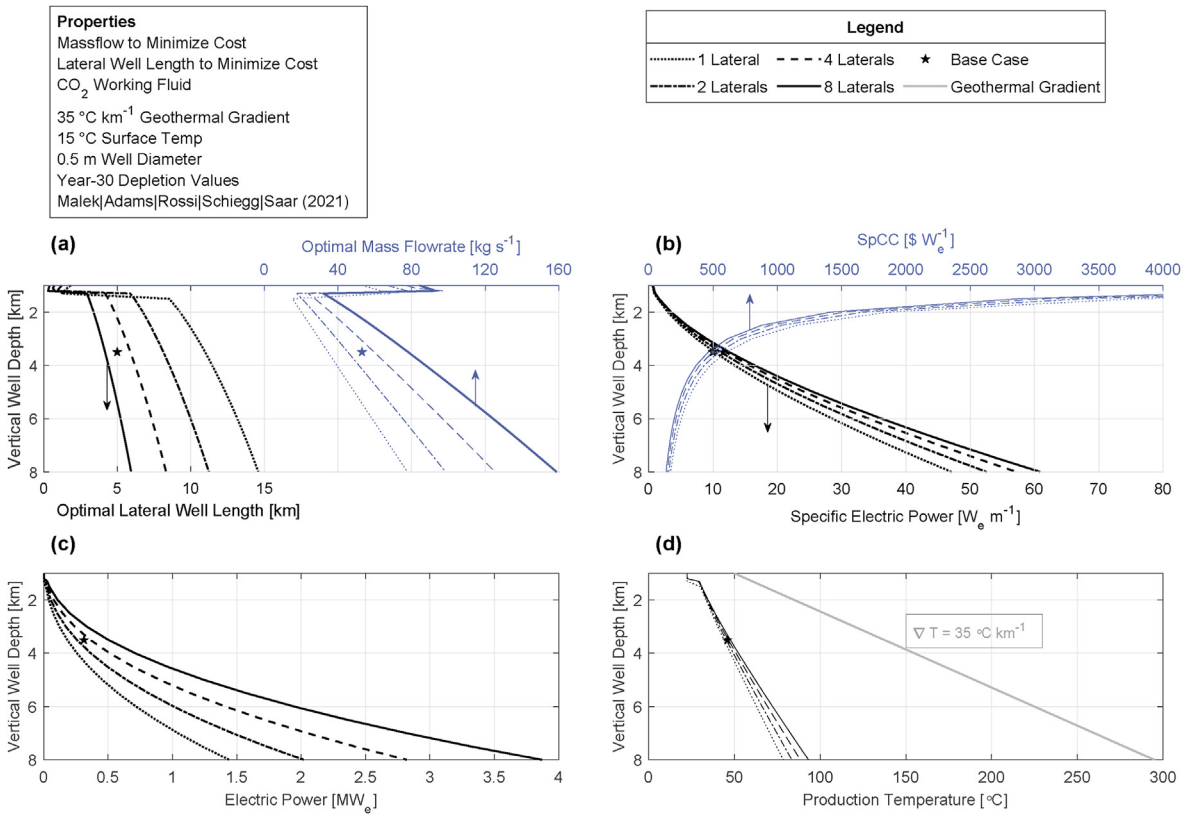


**Fig. 6.** Effect of the number of horizontal lateral wells on AGS performance. The black lines in (a) and (b) correspond to the bottom x-axes of each corresponding plot (denoted by the black arrows) and show the optimal lateral well length and specific electric power, respectively. The blue lines in (a) and (b) correspond to the top x-axis of each corresponding plot (denoted by the blue arrows) and show the optimal mass flowrate, $\dot{m}^*$, and SpCC, respectively. (c) shows the results for electric power. (d) shows the working fluid production temperature (black lines) and the temperature of the surrounding rock (solid gray line) considering a geothermal gradient, $\nabla T$, of 35 °C km$^{-1}$. The stars indicate the outputs from the base case.

## 4. Discussion

In this section, we elaborate on the results of the parametric study by providing a more detailed quantitative analysis and by discussing the observed trends. Thereafter, we provide a more general discussion regarding the costs associated with developing wellbores for AGS, and technological advancements that may reduce them.

### 4.1. Analysis of parametric study

Our results can be used to quantify the operating parameters (i.e., working fluid type, mass flowrates, length and number of horizontal lateral wells, well diameter) and geologic conditions (i.e., geothermal gradient, rock thermal conductivity) that optimize the electricity generation and cost of any AGS development worldwide.

We find that operating the AGS at an optimal working fluid mass flowrate, $\dot{m}^*$, minimizes the SpCC. As shown by Equation (5), the heat flux from the well into the working fluid, $q_{\text{pipe-fluid}}$, depends on the heat exchange characteristics between the surrounding rock and the well, $Q_{\text{rock-pipe}}$, and the working fluid mass flowrate, $\dot{m}$. $Q_{\text{rock-pipe}}$ is a function of the rock thermal conductivity, $k_{\text{rock}}$, and $T_{\text{surrounding}}$, and is thus a constant with time at a given vertical well depth [41]. Mass flowrates that are too high result in insufficient $q_{\text{pipe-fluid}}$ to generate economically viable levels of electric power, thereby rendering the system to be thermally inefficient. Ref. [53] additionally states that the electric power is decreased due to significant amounts of exergy being destroyed from large frictional losses arising from higher mass flowrates. Conversely, mass flowrates that are too low result in low electric power generation due to a low throughput, despite a high production temperature and large $q_{\text{pipe-fluid}}$,

$$q_{\text{pipe-fluid}} \propto \frac{Q_{\text{rock-pipe}}}{\dot{m}}. \tag{5}$$

We also observe that more electric power is generated from using $CO_2$ as the subsurface, closed-loop working fluid, rather than water. This results from system inefficiencies for the water-based system that arise during the heat exchange from the water into the secondary working fluid (here R245fa) in the organic Rankine cycle (ORC). These heat losses do not exist in the $CO_2$-based system, where electricity is generated directly by expanding the $CO_2$ in a turbine (see Fig. 2). Despite generating less power, the working fluid's production temperatures are higher in the water-based system. Studies of other, open-loop (defined in the introduction) geothermal systems (i.e., EGS and CPG) suggest that $CO_2$ has a higher heat extraction efficiency compared to water [20,22,54,55], hence our interest in studying the effect of using $CO_2$ in the closed subsurface loop of AGS.

Other than yielding a higher electric power output, an additional benefit of using $CO_2$ instead of water as a subsurface working fluid is that it reduces, and in some cases eliminates, the pumping power requirements. $CO_2$ has a smaller viscosity than water, which results in less frictional losses within the wellbores and therefore less pumping is required to achieve an equivalent mass flowrate. More

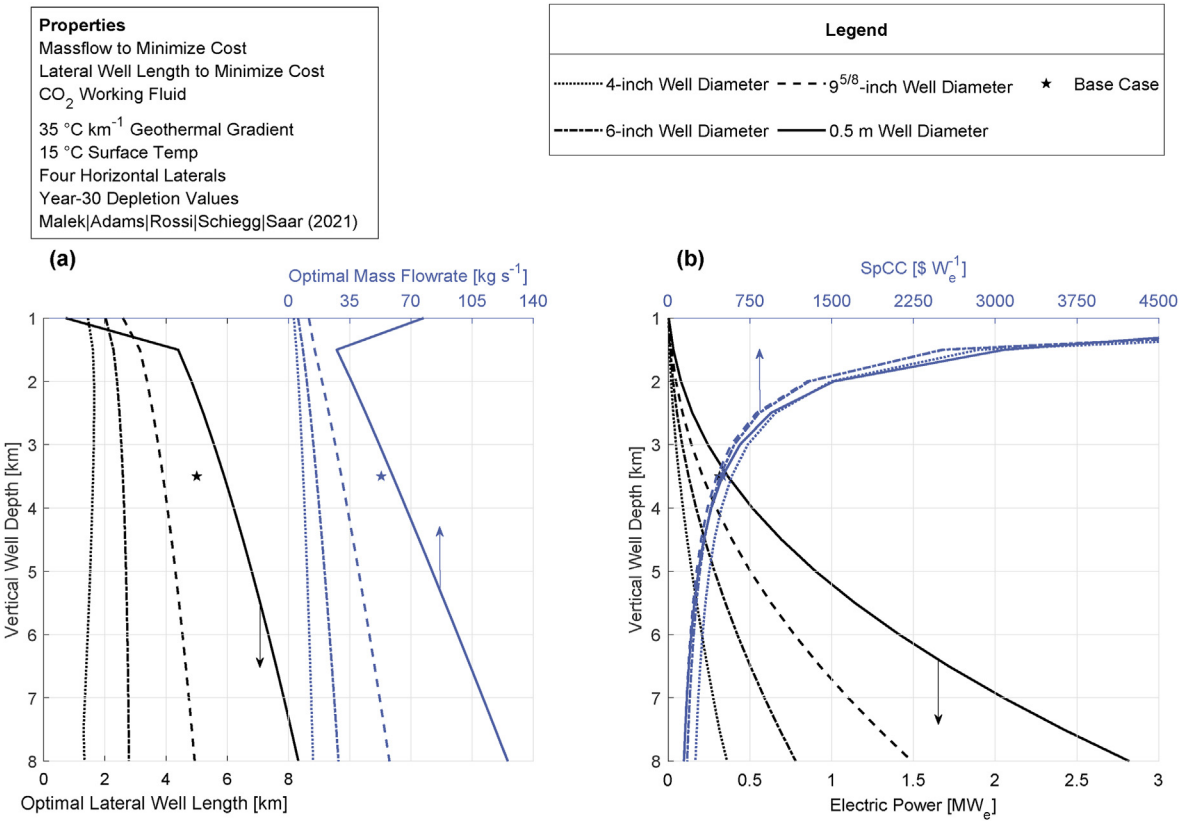


**Fig. 7.** Effect of the well diameter on AGS performance. The black lines (optimal lateral well length in (a) and electric power in (b)) and the blue lines (optimal mass flowrate in (a) and SpCC in (b)) are shown on the bottom and the top x-axes, respectively. The stars indicate the outputs from the base case.

importantly, $CO_2$ has a higher compressibility than water, which results in a density and pressure contrast at the land surface between the low-density, hot $CO_2$ leaving the production well and the high-density, cool $CO_2$ entering the injection well, which tends to drive self-sustained, buoyancy-driven circulation (a thermosiphon) of the working fluid [21,56–58]. Conversely, the density and pressure contrast at the land surface is small for water. This is evident in Fig. 10a, where the land surface pressure difference for the 3.5 km deep $CO_2$ system is 4.9 MPa and only 0.6 MPa for the water system. In typical geothermal cases, the surface pressure differential is insufficient to circulate water, thus pumping is required. Therefore, the genGEO software allows for the use of a downhole pump in the water-based system. However, the 0.6 MPa pressure difference in the water-based system (under base-case operating conditions) is sufficient to drive a thermosiphon without requiring any pumping.

Fig. 10 shows the working fluid temperature and pressure profiles for an AGS with vertical well depths that extend down to 3.5 km (base-case) and 8.0 km. The working fluids descend down the injection well (states 1–2), through four lateral wells (states 2–3), and up the production well (states 3–4), where state 4 is the production temperature and pressure. The rock temperature, resulting from the 35 °C $km^{-1}$ geologic temperature gradient is shown as the solid gray line.

The temperature change in the vertical wells with the $CO_2$ working fluid (black lines) is higher than in the case with water (blue lines). This is due to the previously mentioned high compressibility of $CO_2$, which allows its density to vary significantly within the vertical wellbores (a detailed explanation can be found in Ref. [21]).

Furthermore, the overall temperature change for both fluids is the highest within the horizontal lateral wells. This is caused by the lower fluid velocity in each of the lateral wells (and therefore a higher $q_{\text{pipe-fluid}}$ value), since the mass flowrate is divided by the number of horizontal lateral wells. Thus, a greater number of lateral wells results in a larger overall temperature change and therefore higher electric power generation (see Fig. 6).

The conductive heat flux between the pipe and the surrounding rock, $Q_{\text{rock-pipe}}$, plays a key role in increasing the electric power generated by an AGS. Any increase in well lengths, the number of lateral wells, and the well diameter increases the total surface area over which the pipe is exposed to $Q_{\text{rock-pipe}}$. Additionally, larger vertical well depths and higher geothermal gradients result in hotter far-field rock temperatures, $T_{\text{surrounding}}$, in which the lateral wells are embedded, which increases $Q_{\text{rock-pipe}}$ directly. All these changes result in higher electric power generated by the AGS.

However, varying the operating parameters to maximize the electric power does not necessarily imply a lower SpCC. Although increasing the lateral well length, $L_{\text{LW}}$, increases the electric power generated, Fig. 5a illustrates that it does not lead to a decrease in the SpCC if the lateral well length exceeds the optimal value, $L^*_{\text{LW}}$. This is because longer lateral wells are more expensive to develop. At lateral well lengths longer than $L^*_{\text{LW}}$, the increase in electric power is insufficient to offset the capital cost associated with increasing $L_{\text{LW}}$ any further. Similarly, Fig. 7b shows that increasing the wellbore diameter likewise does not necessarily translate to a decrease in the SpCC. Rather, we find that smaller well diameters are preferred if the wellbores are limited to shallow vertical well depths, where $Q_{\text{rock-pipe}}$ is small. For an AGS with a vertical well depth of 3.5 km, the SpCC reduces from 224 to 154 $\$\,W_e^{-1}$ when decreasing the well diameter from 0.50 m to $9^{5/8}$ inches. Conversely, larger-diameter wellbores are preferred for deeper

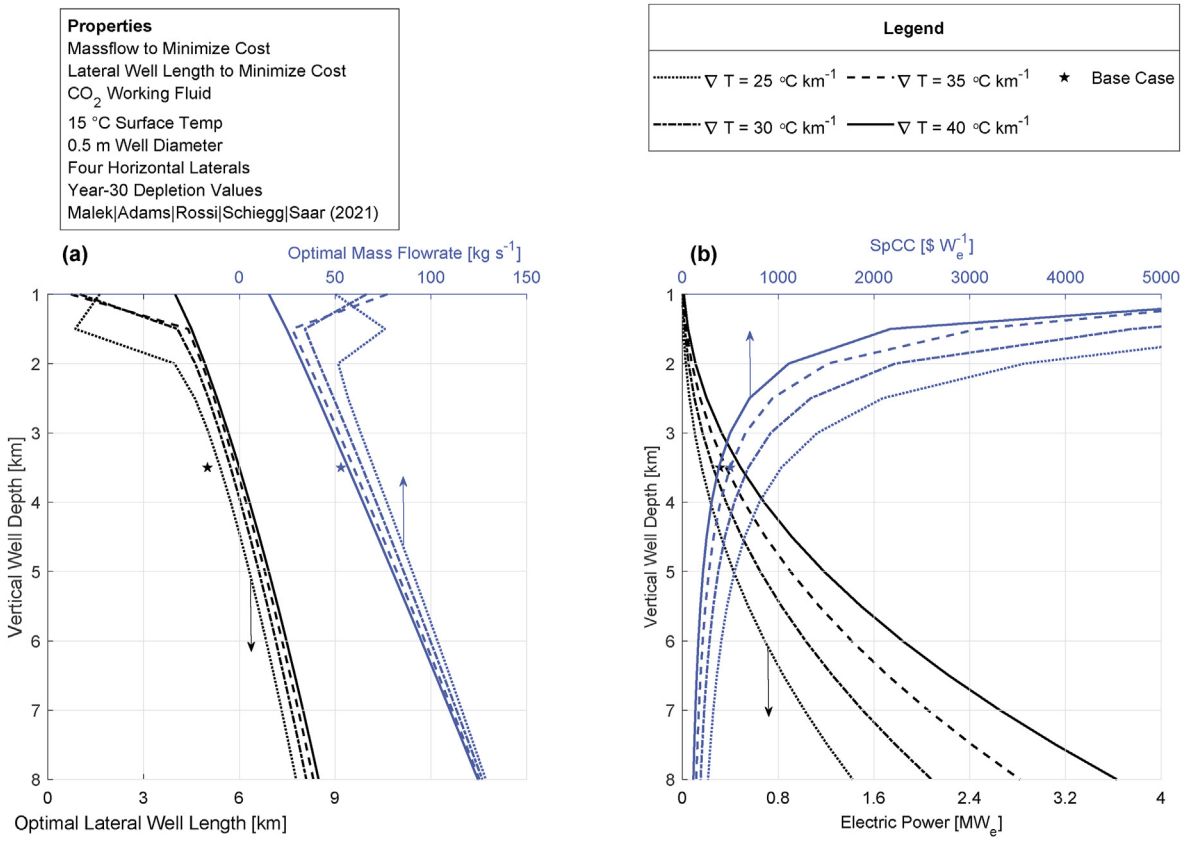


**Fig. 8.** Effect of geological temperature (or geothermal) gradient, $\nabla T$, on AGS performance. The black lines (optimal horizontal lateral well length in (a) and electric power in (b)) and the blue lines (optimal mass flowrate in (a) and SpCC in (b)) are shown on the bottom and the top x-axes, respectively. The stars indicate the outputs from the base case.

installations, where $Q_{\text{rock-pipe}}$ is large. This is a result of the fact that the drilling and completion costs increase with well diameter. Thus, at shallower depths, the increase in electric power produced from using a 0.50 m well is insufficient to offset the higher capital costs associated with the larger well diameter.

In practical situations, where the location of a potential AGS development is given, only the vertical well length, well diameter, and the number of lateral wells can be controlled to optimize the electric power and SpCC. Table 4 shows how the capital costs and SpCC values are affected by these operating parameters.

Table 4 shows that increasing the vertical well depth plays a critical role in decreasing the cost of AGS. Increasing the vertical well depth from 3.5 to 8.0 km, results in a 70% and 77% decrease in 'baseline' and 'ideal' SpCC values, respectively, regardless of the number of lateral wells or well diameters used. This is because the electric power generated by the system is increased significantly. Thus, AGS is more economical when the vertical well depths are large. Unfortunately, drilling through hard crystaline rocks to great depths is difficult with current state-of-the-art drilling technology [35,36]. Additionally, the difference between the 'ideal' and the 'baseline' costs are more significant at greater depths. Therefore, advancements in drilling technology, which render well development more affordable, are urgently needed if AGS are to become economically viable.

Table 5 illustrates the effect that increasing the vertical well depth has on the variation in electric power and SpCC among the several well diameters and number of lateral wells investigated in Section 3. When considering ideal lateral well lengths, the factor by which electric power increases and SpCC decreases, as a response to increasing the number of lateral wells, is independent of the vertical well depth. The electric power increases on average by 63% and the SpCC decreases by 22%. However, the magnitude by which the SpCC decreases is more pronounced at shallower vertical well depths. For example, changing the number of horizontal lateral wells from 1 to 8 at a 3.5 km vertical well depth results in the SpCC decreasing from 12′300 to 9′440 $\$\,W_e^{-1}$, and at an 8.0 km vertical well depth, the SpCC decreases from 3′470 only to 2′750 $\$\,W_e^{-1}$. In contrast, the variation in electric power and SpCC among the well diameters considered in this study increases notably with vertical well depth. Thus, determining the power-maximizing well diameter versus the cost-minimizing well diameter is imperative to successfully design deep AGS installations that yield the desired performance parameters.

To investigate the effect of the geologic conditions on the AGS performance, we perform sensitivity analyses on a wide range of geothermal gradients and rock thermal conductivities, $k_{\text{rock}}$ (see Sections 3.5 to 3.6). Increasing these conditions increases $Q_{\text{rock-pipe}}$ directly, however, the former has a greater effect on the AGS electric power output. At a depth of 3.5 km, decreasing the geothermal gradient and $k_{\text{rock}}$ by 25% (from 40 to 30 °C km$^{-1}$ and from 2.8 to 2.1 $W_{th}$°C$^{-1}$ m$^{-1}$), the electric power generated is reduced by 47% and 22%, respectively. Additionally, Table 6 shows that the degree by which the electric power and SpCC change, due to a change in geothermal gradient, is more pronounced at larger vertical well depths. In contrast, at any vertical well depth, the electric power and SpCC vary by 34% and 36%, respectively, for the range of thermal conductivity values investigated in this paper.

AGS is not restricted only to geothermally active regions. Geologic temperature gradients of 25–40 °C km$^{-1}$ are investigated

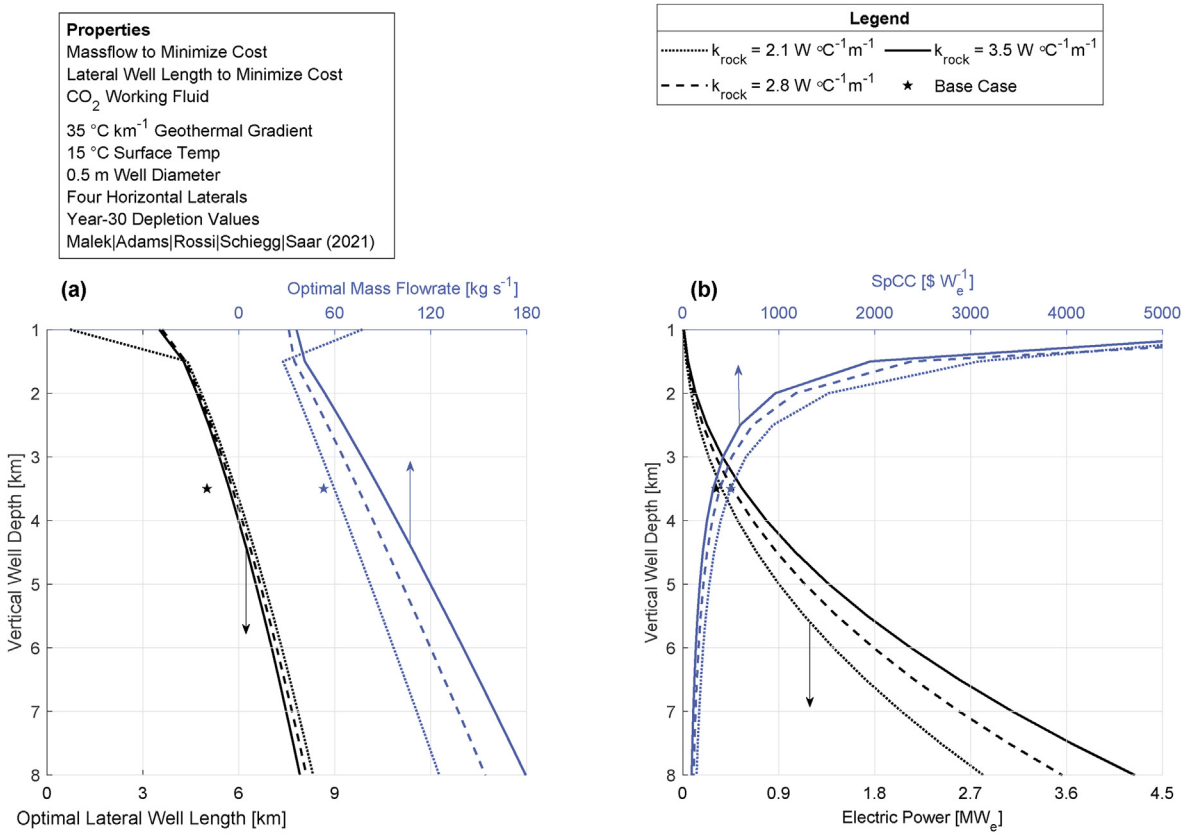


**Fig. 9.** Effect of the rock thermal conductivity, $k_{rock}$, on AGS performance. The black lines (optimal lateral well length in (a) and electric power in (b)) and the blue lines (optimal mass flowrate in (a) and SpCC in (b)) are shown on the bottom and the top x-axes, respectively. The stars indicate the outputs from the base case.

in this study as they are representative of average global values for Earth's continental crust. The average geothermal gradient is 34 °C km$^{-1}$ in the western United States [43], and ranges between 25 and 40 °C km$^{-1}$ in western Canada [59,60], rarely exceeding the latter value. Although high geothermal gradients benefit AGS performance, Fig. 8b shows that AGS are still found to generate 1422 kW$_e$ for 8 km deep wells, which are exposed to 25 °C km$^{-1}$ geothermal temperature gradients.

### 4.2. Cost analysis

Levelized cost metrics, such as the Levelized Cost of Electricity (LCOE), depend on several financing assumptions, and may thus often be misleading. Such financing assumptions (i.e., a discount (i.e., interest) rate for system financing or expected life-cycle production costs) are often very subjective, yet are critical when evaluating renewable energy technologies [61]. Additionally, levelized cost metrics cannot be used to compare intermittent power-generating technologies (i.e., wind and solar) to a dispatchable power-generating technology [62], such as AGS. We thus use the specific capital cost (SpCC) as the cost metric in this study, as it avoids having to make such far-reaching financial assumptions. Thus, we believe that the SpCC is the most objective measure when comparing widely different types of power plants. By applying appropriate financing assumptions, the SpCC can be converted to an LCOE [38].

Wellbore drilling and completion costs comprise the majority of the total AGS capital cost. This is a consequence of the fact that AGS requires drilling to very large depths, typically in hard, crystalline rocks, and drilling costs tend to increase exponentially with depth [63]. Drilling to great depths in hard rock is challenging due to drill speed, i.e., rate of penetration (ROP), issues [49], potentially significant loss of circulating drilling fluid [64], as well as high casing and cementing costs. Both 'baseline' and 'ideal' drilling cost models assume rotary drilling techniques and fully-cased wellbores (both horizontal and vertical). Fig. 11 shows that for a 3.5 km-deep AGS, with four 5.0 km-long lateral wells and a $9^{5/8}$-inch well diameter, well drilling accounts for 95% of the total capital cost of 109 M$. The other capital costs include the wellfield development costs (1.5 M$), gathering system costs (1.0 M$), and the surface power plant development costs (3.1 M$). The total capital cost amounts to 34 M$, 84% of which are the well drilling costs if 'ideal' well costs are assumed. Clearly, advancements in drilling technologies are critical in reducing the capital costs of all geothermal power plant systems [34,63], as this would significantly reduce much of the financial barriers associated with AGS, currently rendering AGS uneconomical.

Elimination of the casing within the horizontal lateral wells (and possibly vertical wells) would contribute to further reductions in the capital costs. The material costs related to well casing (metal, cementing) accounts for up to 60% of the total well development cost [48]. The absence of a casing in the lateral wells is possible, provided that the fluid pressures within these wells are large enough to prevent the wellbore from collapsing, which should be further investigated in future research.

More efficient drilling methods with alternative rock-breaking mechanisms, as opposed to standard 'rotary' techniques, will further reduce costs. Such methods are currently being investigated and include different contact-less approaches, such as plasma [65–69], electric impulse [70–73], laser [74,75], and thermal

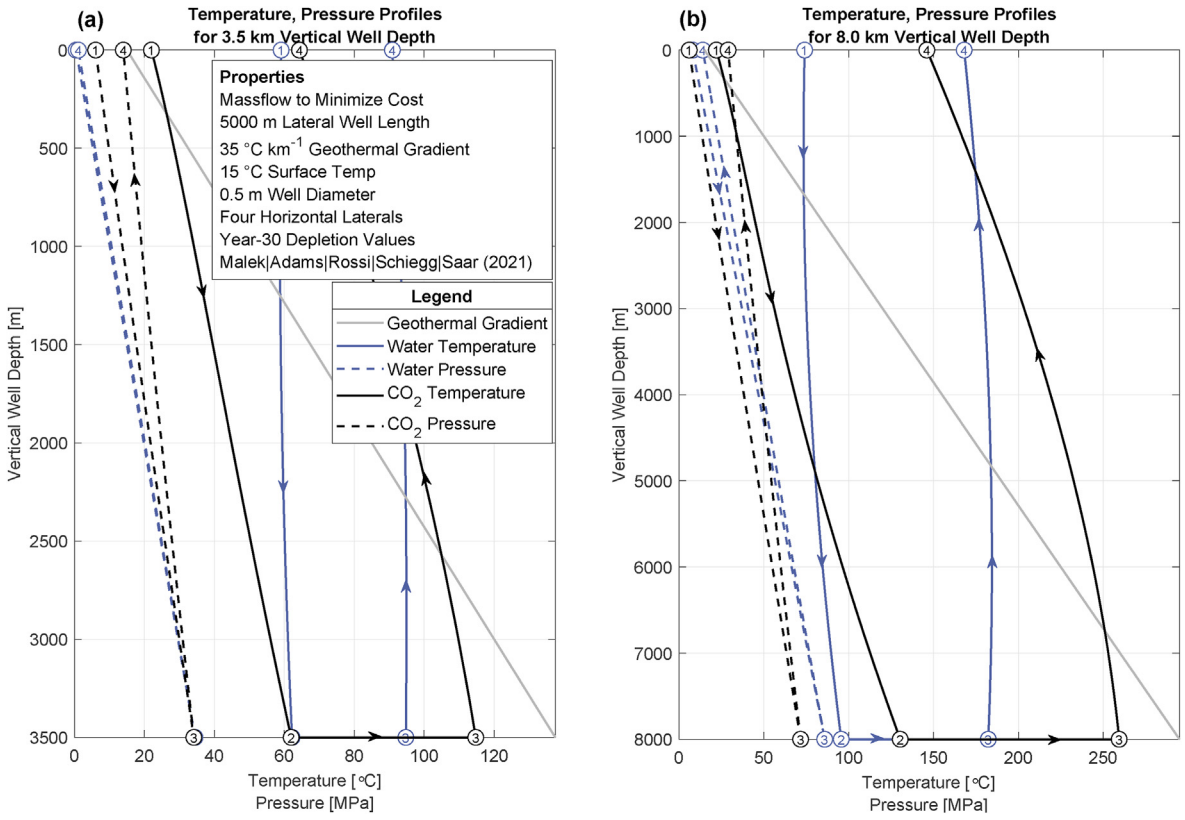


**Fig. 10.** Temperature and pressure profiles for water (blue lines) or $CO_2$ (black lines) as the subsurface, closed-loop working fluid in AGS. The working fluid's direction of travel in the subsurface is indicated by the arrows. The working fluid descends down the injection well (states 1–2) to a vertical depth of (a) 3.5 km or (b) 8.0 km. It then travels horizontally through four lateral wells (states 2–3), to the production well which brings it back to the surface (states 3–4). The pressure change in the horizontal lateral wells is minimal and therefore points 2 and 3 overlay one another. The geothermal gradient, $\nabla T$, is shown by the gray line and represents the temperature of the rock surrounding the well at the corresponding depth.

**Table 4**
Electric power, 'baseline' SpCC, and, in brackets, 'ideal' SpCC comparison for different vertical well depths, well diameters, and number of horizontal lateral wells. The results are shown for 5 km-long lateral wells and a geothermal gradient of 35 °C $km^{-1}$. The starred parameters result in cost-minimization when compared to the alternative option.

| **Vertical Well Depth[km]** | Well diameter | Number of lateral wells | Electric Power [$kW_e$] | Capital Cost [M$] | SpCC [$\$ W_e^{-1}$] |
|---|---|---|---|---|---|
| **3.5** | $9^{5/8}$-inch* | 1 | 85 | 47 (20) | 557 (236) |
| | | 4* | 259 | 116 (40) | 450 (154) |
| | 0.50 m | 1 | 99 | 64 (33) | 656 (339) |
| | | 4* | 313 | 156 (70) | 499 (224) |
| **8.0*** | $9^{5/8}$-inch* | 1 | 625 | 109 (34) | 174 (53) |
| | | 4* | 1505 | 219 (55) | 145 (37) |
| | 0.50 m | 1 | 742 | 140 (57) | 188 (77) |
| | | 4* | 1845 | 273 (96) | 147 (52) |

**Table 5**
Variation in electric power and specific capital cost (SpCC) for various well diameters and number of horizontal lateral wells, at each 1 km depth increment for vertical well depths between 2 and 8 km.

| | **Well Diameters** | | **Number of Lateral Wells** | |
|---|---|---|---|---|
| Depth [km] | Variation in Electric Power | Variation in 'baseline' SpCC | Variation in Electric Power | Variation in 'baseline' SpCC |
| 2 | 78% | 16% | 64% | 24% |
| 3 | 80% | 21% | 64% | 24% |
| 4 | 82% | 26% | 64% | 23% |
| 5 | 84% | 31% | 63% | 22% |
| 6 | 85% | 35% | 63% | 22% |
| 7 | 87% | 39% | 63% | 21% |
| 8 | 87% | 42% | 63% | 21% |

**Table 6**
Variation in electric power and specific capital cost (SpCC) for various geothermal gradients (25–40 °C km$^{-1}$) and rock thermal conductivities (2.1–3.5 W$_{th}$°C$^{-1}$m$^{-1}$), at each 1 km depth increment for vertical well depths between 2 and 8 km.

| | Geothermal Gradient | | Rock Thermal Conductivity | |
|---|---|---|---|---|
| Depth [km] | Variation in Electric Power | Variation in 'baseline' SpCC | Variation in Electric Power | Variation in 'baseline' SpCC |
| 2 | 75% | 69% | 35% | 36% |
| 3 | 69% | 65% | 35% | 36% |
| 4 | 66% | 62% | 34% | 36% |
| 5 | 64% | 60% | 34% | 36% |
| 6 | 63% | 59% | 34% | 36% |
| 7 | 62% | 58% | 34% | 36% |
| 8 | 61% | 57% | 34% | 36% |

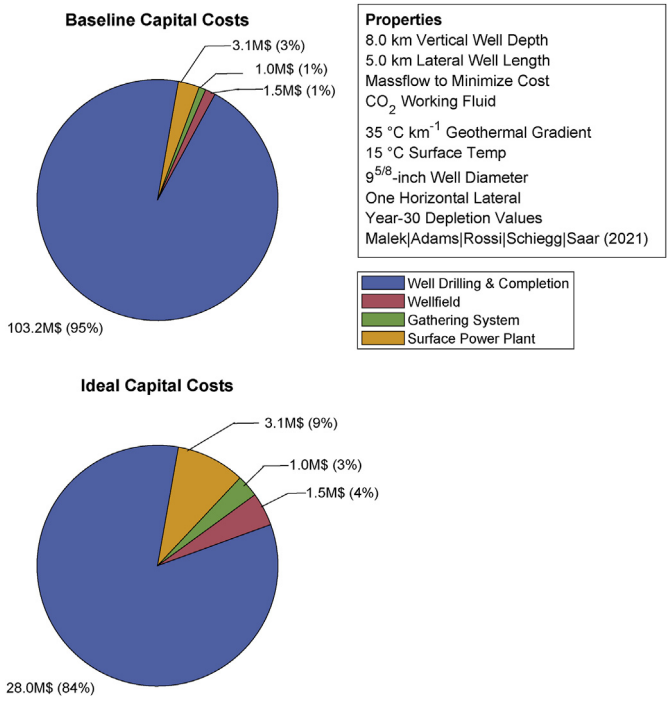


**Fig. 11.** 'Baseline' and 'ideal' capital costs for all AGS components.

spallation [76–78] drilling as well as combined thermo-mechanical drilling (CTMD) concepts [79,80].

Other technological improvements to drilling, that would reduce AGS costs, relate to deep well drilling, directional drilling, wellbore geomechanics and well completion, which has been well-documented by Ref. [29].

Although this paper uses the SpCC as the main metric to assess AGS performance, the evaluation of optimal investments must also incorporate the several societal benefits arising from renewable power generation [81], in particular by AGS. If properly implemented, AGS would benefit society by producing no greenhouse gas (GHG) emissions, while providing carbon-free dispatchable power that would allow a reliable supply of baseload electricity (and/or heat) without the need for energy storage. Currently a multitude of methods exist that can be used to quantify the monetary impact of societal benefits, such as using social discount rates [82]. These societal benefits increase the welfare of present and future generations and society's willingness to pay for power generation from such systems [83].

## 5. Conclusions

This work presents novel results that can be used to evaluate the performance of Advanced Geothermal Systems (AGS). AGS performance is expressed through the electric power and specific capital cost (SpCC) generated after simulating AGS employing the genGEO techno-economic simulator. The methodology outlined in this study can be applied to any AGS worldwide, with the aim of assisting the economic feasibility assessments of these systems.

In addition, a parametric analysis is done by simulating the 30-year AGS performance to determine the operating parameters and geologic conditions which favor cost-minimization of the AGS. The main findings of the parametric analysis can be summarized as follows:

(1) *Utilizing $CO_2$, instead of water, as the subsurface working fluid in a closed-loop, i.e., heat-conduction-dominated, system, results in a higher electric power output and in lower costs in all the cases examined in this study.* System inefficiencies in the water system, arising from the heat transfer to a secondary Rankine cycle, causes the water-based system to generate less power than the $CO_2$-based system. A $CO_2$-based geothermal system is essentially a (single) power cycle in-and-of itself, thereby eliminating these heat losses.

(2) *An optimal fluid mass flowrate, which results in minimized costs, exists for any given set of system parameters.* High fluid mass flowrates result in insufficient conductive heat fluxes from the rock formation to the working fluid in the closed loop. This impedes economical (electric) power generation. Likewise, low fluid mass flowrates generate little electric power due to a low throughput, despite resulting in a higher heat flux. Therefore, the optimal fluid mass flowrate is a balance among the aforementioned factors.

(3) *An optimal lateral well length, minimizing costs, exists for any given set of system parameters.* Well costs increase non-linearly with depth, and long wells, while increasing the production temperature, are also expensive. Thus, the optimal lateral well length balances well costs with electricity generation efficiency.

(4) *Increasing the number of horizontal lateral wells increases the electric power produced by the AGS and decreases its specific capital cost (SpCC).* When the number of lateral wells increases from 1 to 8, the electric power increases by approximately 63% and the SpCC decreases by approximately 22% for any vertical well depth. However, the production temperature stays constant regardless of the number of lateral wells installed.

(5) *An optimal wellbore diameter, minimizing costs, exists for any given set of system parameters.* Smaller well diameters are preferred at shallower depths, where the heat flux into the pipe is small. Conversely, at greater depths, increasing the well diameter to larger sizes benefits the system by lowering the SpCC.

(6) *Installing AGS in geothermally active zones, characterized by larger geothermal gradients, greatly benefits the AGS performance, however, it is not necessary for successful system operation.* An 8.0 km deep AGS installation, with four 5.0 km-long lateral wells in a low 25 °C km$^{-1}$ region, generates 1422 kW$_e$. This power output is increased to 3629 kW$_e$ if the geothermal gradient is 40 °C km$^{-1}$.

(7) *AGS is significantly more economical when the vertical wells are deeper.* For an AGS with 5.0 km-long lateral wells, increasing the vertical well depth from 3.5 km to 8.0 km reduces the SpCC by over 70% (Table 4).

Our findings equitably show that with current drilling technologies, AGS are economically non-viable, as the 'baseline' SpCC values are significantly above the 2.0–5.0 2019$\$W_e^{-1}$ range typically considered economical [37]. We argue that these costs can be reduced with technological advancements. Developing an 8.0 km-deep AGS with state-of-the-art drilling technologies with four 5.0 km-long horizontal lateral wells and well diameters of $9^{5/8}$ inches results in an SpCC of 145 $\$W_e^{-1}$ (Table 4). This SpCC is reduced to 37 $\$W_e^{-1}$ if significant advancements of the current state-of-the-art drilling technologies were to occur that would validate the use of the 'ideal' cost assumptions. These costs can be further reduced if new drilling methods, with alternative rock-breaking mechanisms (e.g., plasma-pulse geo-drilling (PPGD), electric impulse drilling, thermal spallation drilling, combined thermo-mechanical drilling (CTMD), laser drilling) are developed (for technique citations, see Section 4.2).

The expected external costs of future AGS power plants appear to be negligible as they (1) cause no operational $CO_2$ emissions, (2) use a renewable energy resource (geothermal energy) that enables baseload and dispatchable heat and/or electric power generation and does thus not require power back-up or energy storage infrastructures (3) do not require (e.g., radioactive nuclear), waste storage infrastructures, and (4) can be implemented at small scales, largely independent of the local geology, enabling the deployment of many distributed, autarkic power plants that provide heat and/or electricity to nearby communities without the need for large-scale power lines, while increasing the resilience of the power supply (e.g., reducing the risk of brown/black-outs). Thus, the economic competitiveness of AGS is further significantly increased when the external costs of other power plants (e.g. fossil, nuclear, solar, wind, bio-mass) are considered, for example in full life-cycle analyses (LCA).

## Data and software availability

The power generation and cost data for all cases simulated are provided as supplemental data as an EXCEL file. The most recent version of the genGEO open-source python library can be accessed at: https://github.com/GEG-ETHZ/genGEO.

## CRediT authorship contribution statement

**Adam E. Malek:** Writing – original draft, Software, Visualization, Data curation, Formal analysis. **Benjamin M. Adams:** Software, Writing – review & editing, Resources, Methodology, Conceptualization. **Edoardo Rossi:** Writing – review & editing, Resources. **Hans O. Schiegg:** Funding acquisition, Writing – review & editing. **Martin O. Saar:** Supervision, Funding acquisition, Writing – review & editing.

## Declaration of competing interest

The authors declare that they have no known competing financial interests or personal relationships that could have appeared to influence the work reported in this paper.

## Acknowledgements

The authors gratefully acknowledge funding from Innosuisse (https://www.innosuisse.ch/inno/en/home.html) Grant 28305.1-PFIW-IW. The Werner Siemens Foundation (Werner Siemens-Stiftung – WSS) is further thanked for its support of the Geothermal Energy and Geofluids (GEG) group (https://geg.ethz.ch) at ETH Zurich (ETHZ), Switzerland. We thank the editor for handling the manuscript and the two anonymous reviewers for their excellent feedback on an earlier version of the manuscript, which improved this paper. Any opinions, findings, conclusions, and/or recommendations expressed in this material are those of the authors and do not necessarily reflect the views of Innosuisse, ETHZ, WSS, or SwissGeoPower (SGP).

## Appendix A. Supplementary data

Supplementary data to this article can be found online at https://doi.org/10.1016/j.renene.2022.01.012.

## References

[1] United Nations Framework Convention on Climate Change (UNFCCC), Tech. Rep., in: Adoption of the Paris Agreement, 21st Conference of the Parties, 2015 https://unfccc.int/resource/docs/2015/cop21/eng/l09r01.pdf.
[2] A. Schavan, Germany's Energy Research Plan, Science 330 (6002) (Oct. 2010), https://doi.org/10.1126/science.1198075.
[3] M. Anvari, G. Lohmann, M. Wächter, P. Milan, E. Lorenz, D. Heinemann, M.R.R. Tabar, J. Peinke, Short term fluctuations of wind and solar power systems, New J. Phys. 18 (6) (2016), https://doi.org/10.1088/1367-2630/18/6/063027.
[4] A. Kumar, T. Schei, "Hydropower," in IPCC Special Report on Renewable Energy Sources and Climate Change, Cambridge University Press, Cambridge, United Kingdom and New York, NY, USA, 2011, pp. 437–496, ch. 5.
[5] I. Stober, K. Bucher, Geothermal Energy, Springer Berlin Heidelberg, Berlin, Heidelberg, 2013, https://doi.org/10.1007/978-3-642-13352-7.
[6] E. Huenges, "Enhanced Geothermal Systems," in Geothermal Power Generation, Elsevier, 2016, https://doi.org/10.1016/B978-0-08-100337-4.00025-5.
[7] K. Breede, K. Dzebisashvili, X. Liu, G. Falcone, A systematic review of enhanced (or engineered) geothermal systems: past, present and future, Geoth. Energy 1 (1) (2013) 4, https://doi.org/10.1186/2195-9706-1-4.
[8] S.-M. Lu, A global review of enhanced geothermal system (EGS), Renew. Sustain. Energy Rev. 81 (2018), https://doi.org/10.1016/j.rser.2017.06.097.
[9] E.L. Majer, R. Baria, M. Stark, S. Oates, J. Bommer, B. Smith, H. Asanuma, Induced seismicity associated with enhanced geothermal systems, Geothermics 36 (3) (2007), https://doi.org/10.1016/j.geothermics.2007.03.003.
[10] F. Grigoli, S. Cesca, A.P. Rinaldi, A. Manconi, J.A. López-Comino, J.F. Clinton, R. Westaway, C. Cauzzi, T. Dahm, S. Wiemer, The November 2017 M w 5.5 Pohang earthquake: a possible case of induced seismicity in South Korea, Science 360 (6392) (2018) 1003–1006, https://doi.org/10.1126/science.aat2010.
[11] T. Kraft, P.M. Mai, S. Wiemer, N. Deichmann, J. Ripperger, P. Kästli, C. Bachmann, D. Fäh, J. Wössner, D. Giardini, in: "Enhanced Geothermal Systems: Mitigating Risk in Urban Areas," Eos, vol. 90, Transactions American Geophysical Union, 2009, https://doi.org/10.1029/2009EO320001, 32.
[12] S. Ge and M. O. Saar, "Review: Induced Seismicity during Geoenergy Development - a Hydromechanical Perspective," (Manuscript Submitted for Publication, submitted).
[13] D.D. McNamara, A. Lister, D.J. Prior, Calcite sealing in a fractured geothermal reservoir: insights from combined EBSD and chemistry mapping, J. Volcanol. Geoth. Res. 323 (2016), https://doi.org/10.1016/j.jvolgeores.2016.04.042.
[14] L. Griffiths, M. Heap, F. Wang, D. Daval, H. Gilg, P. Baud, J. Schmittbuhl, A. Genter, Geothermal implications for fracture-filling hydrothermal precipitation, Geothermics 64 (2016) 235–245, https://doi.org/10.1016/j.geothermics.2016.06.006.
[15] J.F. Vernoux, A. Genter, P. Razin, C. Vinchon, Geological and Petrophysical Parameters of a Deep Fractured Sandstone Formation as Applied to Geothermal Exploitation, Tech. Rep. 70, BRGM, 1995, p. 24.
[16] J.L. Ball, P.H. Stauffer, E.S. Calder, G.A. Valentine, The hydrothermal alteration of cooling lava domes, Bull. Volcanol. 77 (12) (2015) 102, https://doi.org/10.1007/s00445-015-0986-z.
[17] S. Regenspurg, E. Feldbusch, J. Byrne, F. Deon, D.L. Driba, J. Henninges, A. Kappler, R. Naumann, T. Reinsch, C. Schubert, Mineral precipitation during production of geothermal fluid from a Permian Rotliegend reservoir, Geothermics 54 (2015) 122–135, https://doi.org/10.1016/j.geothermics.2015.01.003.
[18] V.S. Gischig, D. Giardini, F. Amann, M. Hertrich, H. Krietsch, S. Loew, H. Maurer, L. Villiger, S. Wiemer, F. Bethmann, B. Brixel, J. Doetsch, N.G. Doonechaly, T. Driesner, N. Dutler, K.F. Evans, M. Jalali, D. Jordan, A. Kittilä, X. Ma, P. Meier, M. Nejati, A. Obermann, K. Plenkers, M.O. Saar, A. Shakas, B. Valley, Hydraulic stimulation and fluid circulation experiments in underground laboratories: stepping up the scale towards engineered geothermal systems, Geomech. Energy Environ. 24 (2020), https://doi.org/10.1016/j.gete.2019.100175.
[19] F. Amann, V. Gischig, K. Evans, J. Doetsch, R. Jalali, B. Valley, H. Krietsch, N. Dutler, L. Villiger, B. Brixel, M. Klepikova, A. Kittilä, C. Madonna, S. Wiemer, M.O. Saar, S. Loew, T. Driesner, H. Maurer, D. Giardini, The seismo hydromechanical behavior during deep geothermal reservoir stimulations: open

questions tackled in a decameter-scale in situ stimulation experiment, Solid Earth 9 (1) (2018), https://doi.org/10.5194/se-9-115-2018.
[20] J.B. Randolph, M.O. Saar, Combining geothermal energy capture with geologic carbon dioxide sequestration, Geophys. Res. Lett. 38 (10) (2011), https://doi.org/10.1029/2011GL047265.
[21] B.M. Adams, T.H. Kuehn, J.M. Bielicki, J.B. Randolph, M.O. Saar, On the importance of the thermosiphon effect in CPG (CO2 plume geothermal) power systems, Energy 69 (2014) 409–418, https://doi.org/10.1016/j.energy.2014.03.032.
[22] B.M. Adams, T.H. Kuehn, J.M. Bielicki, J.B. Randolph, M.O. Saar, A comparison of electric power output of CO2 Plume Geothermal (CPG) and brine geothermal systems for varying reservoir conditions, Appl. Energy 140 (2015), https://doi.org/10.1016/j.apenergy.2014.11.043. Feb.
[23] B.M. Adams, D. Vogler, T.H. Kuehn, J.M. Bielicki, N. Garapati, M.O. Saar, Heat depletion in sedimentary basins and its effect on the design and electric power output of CO2 Plume Geothermal (CPG) systems, Renew. Energy 172 (2021), https://doi.org/10.1016/j.renene.2020.11.145.
[24] N. Garapati, B.M. Adams, M.R. Fleming, T.H. Kuehn, M.O. Saar, Combining brine or CO2 geothermal preheating with low-temperature waste heat: a higher-efficiency hybrid geothermal power system, J. CO2 Util. 42 (2020), https://doi.org/10.1016/j.jcou.2020.101323.
[25] S.-Y. Pan, M. Gao, K.J. Shah, J. Zheng, S.-L. Pei, P.-C. Chiang, Establishment of enhanced geothermal energy utilization plans: barriers and strategies, Renew. Energy 132 (2019), https://doi.org/10.1016/j.renene.2018.07.126.
[26] D.W. Brown, Hot dry rock geothermal energy: Important lessons from Fenton Hill, in: Thirty-Fourth Workshop on Geothermal Reservoir Engineering, 2009, pp. 1–6.
[27] W.-L. Cheng, C.-L. Wang, Y.-L. Nian, B.-B. Han, J. Liu, Analysis of influencing factors of heat extraction from enhanced geothermal systems considering water losses, Energy 115 (2016), https://doi.org/10.1016/j.energy.2016.09.003.
[28] A.E. Malek, B.M. Adams, E. Rossi, H.O. Schiegg, M.O. Saar, Electric power generation, specific capital cost, and specific power for advanced geothermal systems (AGS), in: Fourty-Sixth Workshop on Geothermal Reservoir Engineering, 2021, https://doi.org/10.3929/ethz-b-000467172.
[29] E. van Oort, D. Chen, P. Ashok, A. Fallah, Constructing Deep Closed-Loop Geothermal Wells for Globally Scalable Energy Production by Leveraging Oil and Gas ERD and HPHT Well Construction Expertise, SPE, Mar, 2021, https://doi.org/10.2118/204097-MS.
[30] X. Song, Y. Shi, G. Li, Z. Shen, X. Hu, Z. Lyu, R. Zheng, G. Wang, Numerical analysis of the heat production performance of a closed loop geothermal system, Renew. Energy 120 (2018) 365–378, https://doi.org/10.1016/j.renene.2017.12.065.
[31] M. Esmaeilpour, M. Gholami Korzani, T. Kohl, Performance analyses of deep closed-loop U-shaped heat exchanger system with a long horizontal extension, in: Forty-Sixth Workshop on Geothermal Reservoir Engineering, 2021, pp. 1–8.
[32] F. Sun, Y. Yao, G. Li, X. Li, Geothermal energy development by circulating CO2 in a U-shaped closed loop geothermal system, Energy Convers. Manag. 174 (2018) 971–982, https://doi.org/10.1016/j.enconman.2018.08.094. July.
[33] G. Wang, X. Song, Y. Shi, R. Yang, F. Yulong, R. Zheng, J. Li, Heat extraction analysis of a novel multilateral-well coaxial closed-loop geothermal system, Renew. Energy 163 (2021) 974–986, https://doi.org/10.1016/j.renene.2020.08.121.
[34] D.A. Blankenship, J.L. Wise, S.J. Bauer, A.J. Mansure, R. Normann, D. Raymond, R. LaSala, Research efforts to reduce the cost of well development for geothermal power generation, in: 40th U.S. Symposium on Rock Mechanics (USRMS), 2005, p. 10.
[35] M.B. Diaz, K.Y. Kim, T.-H. Kang, H.-S. Shin, Drilling data from an enhanced geothermal project and its pre-processing for ROP forecasting improvement, Geothermics 72 (2018), https://doi.org/10.1016/j.geothermics.2017.12.007.
[36] H. Fay, Practical evaluation of rock-BitWearWhile drilling, SPE Drill. Complet. 8 (1993), https://doi.org/10.2118/21930-PA.
[37] IRENA, Renewable Power Generation Costs in 2019, International Renewable Energy Agency, Abu Dhabi, Tech, 2020. Rep.
[38] B. M. Adams, J. D. Ogland-Hand, J. M. Bielicki, P. Schaedle, and M. O. Saar, "Estimating the Geothermal Electricity Generation Potential of Sedimentary Basins Using genGEO (The Generalizable GEOthermal Techno-Economic Simulator)," Manuscript Submitted for Publication, submitted. doi: 10.26434/chemrxiv.13514440.v1.
[39] K.F. Beckers, K. McCabe, GEOPHIRES v2.0: updated geothermal techno-economic simulation tool, Geoth. Energy 7 (1) (2019), https://doi.org/10.1186/s40517-019-0119-6.
[40] Steven CJ. Hanson, Geothermal Electricity Technology Evaluation Model (GETEM) Individual Case Files and Summary Spreadsheet (GETEM Version Spring 2013), Idaho Falls, Idaho, USA, 2013, https://doi.org/10.15121/1148822.
[41] Y. Zhang, L. Pan, K. Pruess, S. Finsterle, A time-convolution approach for modeling heat exchange between a wellbore and surrounding formation, Geothermics 40 (4) (2011) 261–266, https://doi.org/10.1016/j.geothermics.2011.08.003.
[42] F.F. Farshad, H.H. Rieke, Surface roughness design values for modern pipes, SPE Drill. Complet. 21 (2006), https://doi.org/10.2118/89040-PA, 03, Sep.
[43] M. Nathenson, M. Guffanti, Geothermal gradients in the conterminous United States, J. Geophys. Res. 93 (1988), https://doi.org/10.1029/JB093iB06p06437. B6.
[44] G.R. Beardsmore, J.P. Cull, Crustal Heat Flow, Cambridge University Press, 2001, https://doi.org/10.1017/CBO9780511606021. Aug.
[45] D.W. Waples, J.S. Waples, A review and evaluation of specific heat capacities of rocks, minerals, and subsurface fluids. Part 1: minerals and nonporous rocks, Nat. Resour. Res. 13 (2) (2004), https://doi.org/10.1023/B:NARR.0000032647.41046.e7.
[46] S.B. Smithson, Densities of metamorphic rocks, Geophysics 36 (4) (1971), https://doi.org/10.1190/1.1440205. Aug.
[47] H. Carslaw, J. Jaeger, Conduction of Heat in Solids, second ed., Oxford University Press, London, 1959.
[48] T.S. Lowry, J.T. Finger, C.R. Carrigan, A. Foris, M.B. Kennedy, T.F. Corbet, C.A. Doughty, S. Pye, E.L. Sonnenthal, GeoVision Analysis: Reservoir Maintenance and Development Task Force Report (GeoVision Analysis Supporting Task Force Report : Reservoir Maintenance and Development), Tech. Rep., Sandia National Laboratories (SNL), Albuquerque, NM, and Livermore, CA (United States), Sep. 2017, https://doi.org/10.2172/1394062.
[49] J.T. Finger, D.A. Blankenship, Handbook of Best Practices for Geothermal Drilling, Sandia National Laboratories (SNL), 2012, https://doi.org/10.2172/1325261. Albuquerque, NM, and Livermore, CA (United States), Tech. Rep.
[50] C. Teodoriu, G. Falcone, Comparison of well completions used in oil/gas production and geothermal operations: a new approach to technology transfer, in: Thirty-Third Workshop on Geothermal Reservoir Engineering, 2008.
[51] K. Ragnars, S. Benediktsson, Drilling of a 2000 m Borehole for Geothermal Steam in Iceland, Tech. Rep., National Energy Authority of Iceland, 1981 https://www.osti.gov/biblio/7369364-drilling-ft-borehole-geothermal-steam-iceland.
[52] K. Williamson, R. Gunderson, G. Hamblin, D. Gallup, K. Kitz, Geothermal power technology, IEEE 89 (12) (2001) 1783–1792.
[53] A.P. Davis, E.E. Michaelides, Geothermal power production from abandoned oil wells, Energy 34 (7) (2009), https://doi.org/10.1016/j.energy.2009.03.017. Jul.
[54] K. Pruess, N. Spycher, Enhanced geothermal systems (EGS) with CO2 as heat transmission fluid - a Scheme for combining recovery of renewable energy with geologic storage of CO2, in: World Geothermal Congress, April 25 - 29, Bali, Indonesia, 2010.
[55] K. Pruess, Enhanced geothermal systems (EGS) using CO2 as working fluid—a novel approach for generating renewable energy with simultaneous sequestration of carbon, Geothermics 35 (4) (2006), https://doi.org/10.1016/j.geothermics.2006.08.002. Aug.
[56] D.W. Brown, A hot Dry rock geothermal energy concept utilizing supercritical CO2 instead of water, in: Twenty-Fifth Workshop on Geothermal Reservoir Engineering, 2000, pp. 233–238.
[57] A.D. Atrens, H. Gurgenci, V. Rudolph, CO $_2$ thermosiphon for competitive geothermal power generation, Energy Fuels 23 (1) (2009), https://doi.org/10.1021/ef800601z.
[58] A.D. Atrens, H. Gurgenci, V. Rudolph, Electricity generation using a carbon-dioxide thermosiphon, Geothermics 39 (2) (2010), https://doi.org/10.1016/j.geothermics.2010.03.001.
[59] J. Majorowicz, M.J. Unsworth, T. Chacko, D.A. Gray, L.M. Heaman, D.K. Potter, D.R. Schmitt, T. Babadagli, Geothermal energy as a source of heat for oil sands processing in Northern Alberta, Canada, in: F.J. Hein, D. Leckie, S. Larter, J.R. Suter (Eds.), Heavy-Oil and Oil-Sand Petroleum Systems in Alberta and beyond: AAPG Studies in Geology, vol. 64, AAPG, 2013, pp. 725–746.
[60] C. Hickson, K. Huang, D. Cotteril, W. Gosnold, D. Benoit, A relook at Canada's western Canada sedimentary basin for power generation and direct-use energy production, in: Geothermal Resource Council 2020 Annual Meeting 44, Geothermal Resource Council, New Jersey, 2020, pp. 845–861.
[61] R.C. Lind, K.J. Arrow, G.R. Corey, P. Dasgupta, A.K. Sen, T. Stauffer, J.E. Stiglitz, J. Stockfisch, Discounting for Time and Risk in Energy Policy, RFF Press, Oct. 2013, https://doi.org/10.4324/9781315064048.
[62] P.L. Joskow, Comparing the costs of intermittent and dispatchable electricity generating technologies, Am. Econ. Rev. 101 (3) (2011), https://doi.org/10.1257/aer.101.3.238.
[63] J.W. Tester, B.J. Anderson, A.S. Batchelor, D.D. Blackwell, R. DiPippo, E.M. Drake, J. Garnish, B. Livesay, M.C. Moore, K. Nichols, S. Petty, M. Nafi Toksoz, R.W. Veatch, R. Baria, C. Augustine, E. Murphy, P. Negraru, M. Richards, Impact of enhanced geothermal systems on US energy supply in the twenty-first century, Phil. Trans. Math. Phys. Eng. Sci. 365 (Apr. 2007), https://doi.org/10.1098/rsta.2006.1964, 1853.
[64] W.A. Nugroho, S. Hermawan, B.H. Lazuardi, R. Mirza, Drilling Problems Mitigation in Geothermal Environment, Case Studies of Stuck pipe and Lost Circulation, SPE, Oct. 2017, https://doi.org/10.2118/186922-MS.
[65] I. Timoshkin, J. Mackersie, and S. MacGregor, "Plasma channel microhole drilling technology," in Digest of Technical Papers. PPC-2003. 14th IEEE International Pulsed Power Conference (IEEE Cat. No.03CH37472), IEEE, pp. 1336–1339. doi: 10.1109/PPC.2003.1278062.
[66] I. Kocis, T. Kristofic, M. Gebura, G. Horvath, M. Gajdos, V. Stofanik, Novel deep drilling technology based on electric plasma developed in Slovakia, in: 2017 XXXIInd General Assembly and Scientific Symposium of the International Union of Radio Science (URSI GASS), IEEE, 2017, https://doi.org/10.23919/URSIGASS.2017.8105224.
[67] E. Rossi, B.M. Adams, D. Vogler, P. Rudolf von Rohr, B. Kammermann, M.O. Saar, Using geologically sequestered CO2 to generate and store geothermal electricity: CO2 plume geothermal (CPG), in: 2nd Applied Energy

Symposium: MIT A+B (MITAB 2020), ETH Zurich, Department of Earth Sciences, Boston, MA, USA, Aug. 2020, https://doi.org/10.3929/ethz-b-000445213, 2020.
[68] M. Ezzat, D. Vogler, B.M. Adams, M.O. Saar, Simulating plasma formation in pores under short electric pulses for plasma pulse Geo Drilling (PPGD), Energies 14 (16) (2021) 4717, https://doi.org/10.3390/en14164717.
[69] M. Ezzat, B. Adams, M.O. Saar, D. Vogler, Numerical Modeling of the Effects of Pore Characteristics on the Electric Breakdown of Rock for Plasma Pulse Geo Drilling, Energies 15 (1) (2022) 250, https://doi.org/10.3390/en15010250.
[70] M. Voigt, E. Anders, F. Lehmann, "Electric Impulse Technology: Less Energy, Less Drilling Time, Less Round Trips," in All Days, SPE, 2016.
[71] E. Anders, F. Lehmann, M. Voigt, Electric impulse technology-long run drilling in hard rocks, in: ASME 2015 34th International Conference on Ocean, Offshore and Arctic Engineering OMAE2015, 2015. May 31-June 5, St. John's, Newfoundland, Canada - OMAE2015-41219.
[72] H.O. Schiegg, A. Rødland, G. Zhu, D.A. Yuen, Electro-pulse-boring (EPB): novel super-deep drilling technology for low cost electricity, J. Earth Sci. 26 (1) (2015) 37–46, https://doi.org/10.1007/s12583-015-0519-x. Feb.
[73] D. Vogler, S.D. Walsh, M.O. Saar, A numerical investigation into key factors controlling hard rock excavation via electropulse stimulation, J. Rock Mech. Geotech. Eng. 12 (4) (2020), https://doi.org/10.1016/j.jrmge.2020.02.002. Aug.
[74] R.A. Parker, B.C. Gahan, R.M. Graves, B. Samih, X. Zhiyue, C.B. Reed, "Laser Drilling: Effects of Beam Application Methods on Improving Rock Removal," in All Days, SPE, 2003, https://doi.org/10.2118/84353-MS. Oct.
[75] S. Jamali, V. Wittig, J. Börner, R. Bracke, A. Ostendorf, Application of high powered Laser Technology to alter hard rock properties towards lower strength materials for more efficient drilling, mining, and Geothermal Energy production, Geomech. Energy Environ. 20 (2019), https://doi.org/10.1016/j.gete.2019.01.001. Dec.
[76] S. Naganawa, Concept of thermal-shock enhanced drill bit for supercritical geothermal drilling, GRC Trans. 41 (2017) 406–417, 2017.
[77] M.A. Kant, E. Rossi, D. Höser, P. Rudolf von Rohr, Thermal spallation drilling , an alternative drilling technology for deep heat mining - performance analysis, cost assessment and design aspects, in: Fourty-Second Workshop on Geothermal Reservoir Engineering, 2017, pp. 1–10.
[78] E. Rossi, S. Jamali, M.O. Saar, P. Rudolf von Rohr, Field test of a combined thermo-mechanical drilling technology. Mode I: thermal spallation drilling, J. Petrol. Sci. Eng. 190 (2020), https://doi.org/10.1016/j.petrol.2020.107005. Jul.
[79] E. Rossi, S. Jamali, D. Schwarz, M.O. Saar, P. Rudolf von Rohr, Field test of a combined thermo-mechanical drilling technology. Mode II: flame-assisted rotary drilling, J. Petrol. Sci. Eng. 190 (2020) 106 880, https://doi.org/10.1016/j.petrol.2019.106880. Jul.
[80] E. Rossi, S. Jamali, V. Wittig, M.O. Saar, P. Rudolf von Rohr, A combined thermo-mechanical drilling technology for deep geothermal and hard rock reservoirs, Geothermics 85 (2020) 101–771, https://doi.org/10.1016/j.geothermics.2019.101771. May.
[81] A. Bergmann, N. Hanley, R. Wright, Valuing the attributes of renewable energy investments, Energy Pol. 34 (9) (2006), https://doi.org/10.1016/j.enpol.2004.08.035. Jun.
[82] A.H. Hermelink, D. Jager, Evaluating our future - the crucial role of discount rates in European Commission energy system modelling. Report of the European Council for an Energy Efficient Economy (ECEEE), Tech. Rep. (2015). https://www.eceee.org/static/media/uploads/site-2/policy-areas/discount-rates/evaluating-our-future-report.pdf.
[83] A. Bastianin, M. Florio, Social cost-benefit analysis of HL-LHC, SSRN Electron. J. (2018), https://doi.org/10.2139/ssrn.3202220.